IMA Journal of Numerical Analysis (2022) **42**, 1665–1699
https://doi.org/10.1093/imanum/drab059
Advance Access publication on 13 August 2021

An HDG method for dissimilar meshes

Manuel Solano*
Departamento de Ingeniería Matemática, Facultad de Ciencias Físicas y Matemáticas and Centro de Investigación en Ingeniería Matemática, Universidad de Concepción, Concepción, Casilla 160-C, Chile
*Corresponding author: msolano@ing-mat.udec.cl

and

Sébastien Terrana, Ngoc-Cuong Nguyen and Jaime Peraire
Department of Aeronautics and Astronautics, Massachusetts Institute of Technology, Cambridge, Massachusetts, MA 02139, USA

[Received on 19 May 2020; revised on 15 March 2021]

We present a hybridizable discontinuous Galerkin (HDG) method for dissimilar meshes. The method is devised by formulating HDG discretizations on separate meshes and gluing these HDG discretizations through appropriate transmission conditions that weakly enforce the continuity of the numerical trace and the numerical flux across the dissimilar interfaces. The transmission conditions are based upon transferring the numerical flux from the first mesh to the second mesh and the numerical trace from the second mesh to the first one. The transfer of the numerical trace/flux from one mesh to the other relies on the extrapolation of the approximate flux, and is made to be consistent with the HDG methodology for conforming meshes. Stability of the HDG method is shown and the error analysis of the HDG method is established. Numerical results are presented to validate the theoretical results.

Keywords: high-order method; nonmatching meshes; noncoincident meshes; dissimilar meshes; hybrid method.

1. Introduction

In different applications, interfaces divide the domain of interest $\Omega \subset \mathbb{R}^d$ ($d = 2, 3$) into several subdomains. For instance, elliptic interface problems (Huynh *et al.*, 2013), where the partial differential equation (PDE) is characterized by jumps of its solution across the interfaces or situations where different PDEs are coupled at the interfaces through different transmission conditions. As the geometrical complexity and the required spatial sampling of the subdomains may be very diverse, it is not uncommon to mesh the subdomains separately, using different meshsizes. For example, in the case of solid–fluid interactions, it is often desirable to have a finer mesh in the region occupied by the fluid, compared with the meshsize of the discretization of the solid. In the literature, it is possible to identify two configurations where the domain of the PDE is discretized on the union of different computational subdomains. In the first one, subdomains are independently meshed to produce *dissimilar meshes* where the interfaces of neighboring subdomains need to be properly 'tied'. This generates gaps and overlaps as depicted in the example shown in Figs 1 and 2. In the second case, the union of different meshes has no gaps and overlaps, but hanging nodes. It results in a nonconforming mesh in which adjacent elements need not share a complete face or edge. The method presented in this manuscript covers both dissimilar meshes and nonconforming meshes.

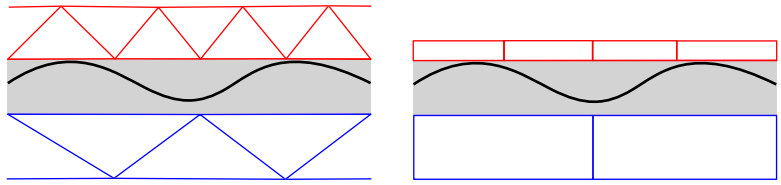

FIG. 1. Example of *dissimilar meshes* in two dimensions made of triangles (left) and quadrilaterals (right). The red mesh is finer than the blue one and the shaded regions (gap) are not meshed. The black solid line is an interface.

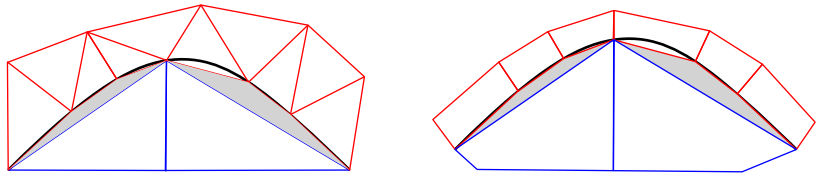

FIG. 2. Similar to Fig. 1, but for the interface (black solid line) is interpolated by both meshes.

A wide variety of methods for piecewise flat interfaces problems can be found in the literature, in contrast to those dealing with curved interfaces. Certainly, in this setting, numerical methods based on finite element approximations are not new. In fact, one of the first approaches in the literature were based on curvilinear maps such as isoparametric finite elements (Bfer, 1985; Lenoir, 1986). The mesh in this type of method is composed by polyhedral partition, where some of the elements have a curved side that interpolates the interface. In general, methods involving curvilinear mappings are computationally expensive because they require to compute nonlinear mappings to construct the basis functions of the discrete spaces associated with the elements near the interface. Moreover, their precision depends on the accuracy of the interpolation spline. In the same direction, isogeometric analysis using NURBS as basis functions can also be used for interface conditions imposing higher-order continuity across the interface (Dittmann *et al.*, 2019).

An alternative to curvilinear methods is to consider polytopal meshes that not necessarily are fitted to the interface. However, the effect of the variational crime of this approach is more significant than that of isoparametric elements. Several methods overcome this lack of accuracy due to the poor approximation of the interface. For example, mortar methods (Flemisch *et al.*, 2005a,b) where a Lagrange multiplier is considered to weakly impose the transmission condition across the curved interface. However, their main drawback is the low-order approximation of the solution. An extension of these mortar methods has been proposed in Flemisch & Wohlmuth (2007). Other approaches perform modifications of the nodes associated with the boundary of the elements near the interface (Dohrmann *et al.*, 2000a,b; Heinstein & Laursen, 2003; Laursen & Heinstein, 2003). A review of other computational techniques can be found in Cockburn & Solano (2014).

Recently, a novel approach provides a high-order method for problems involving curved interfaces approximated by polytopal meshes (Chen & Cockburn, 2014). It is based on the polynomial extension finite element method (PE-FEM) originally developed in the context of boundary value problems (Cheung *et al.*, 2020). Roughly speaking, instead of adjusting the mesh to the interface, PE-FEM forces a polynomial extension of the approximate solution to match the prescribed Neumann or Dirichlet boundary condition. Actually, polynomial extensions have also been used during the past decade, mostly in the context of hybridizable discontinuous Galerkin (HDG) methods (Cockburn *et al.*, 2012, 2014;

Cockburn & Solano, 2012; Qiu *et al.*, 2016). There, the polynomial approximation of the gradient of the solution is extended outside the computational domain, whereas the solution is extended by integrating the polynomial approximation of the gradient along *transferring segments* connecting the computational boundary/interface and the boundary/interface of the domain. We consider the latter approach because of its flexibility to deal also with situations where the meshes do not interpolate the interface, as in the case of immerse-type methods. For example, in Fig. 1, both meshes are *far* from the interface.

Based on the transferring technique of Cockburn *et al.* (2012), our work proposes and analyzes a new method to handle dissimilar as in the examples depicted in Figs 1 and 2. For the sake of simplicity of the analysis and the exposition, we consider the following diffusion problem:

$$\boldsymbol{q} + \nabla u = 0 \quad \text{in} \quad \Omega, \tag{1.1a}$$

$$\nabla \cdot \boldsymbol{q} = f \quad \text{in} \quad \Omega, \tag{1.1b}$$

$$u = 0 \quad \text{on} \quad \Gamma := \partial\Omega, \tag{1.1c}$$

where $\Omega \subset \mathbb{R}^d$ $(d = 2, 3)$ is a polyhedral domain, $f \in L^2(\Omega)$ is a given source term, and u and $\boldsymbol{q}$ are the scalar and flux unknowns. Since the focus of the present study is on the discrete interfaces, we will only consider homogeneous Dirichlet boundary conditions on Γ. However, other types of boundary conditions can be also considered without difficulties. Even though this is a simple model, it poses several technicalities for theoretical analysis, which need to be understood before considering more complex problems.

The remainder of the manuscript is organized as follows. In Section 2, we introduce the HDG method for solving (1.1) on dissimilar meshes and the discrete transmission conditions will be explained. Next, we show the stability of the method in Section 3 and present *a priori* error analysis in Section 4. Finally, numerical results are presented in Section 5 to validate the theoretical results, and conclusions are presented in Section 6.

2. The method

2.1 *Notation*

The computational domain. The physical domain Ω consists of two disjoint open subdomains Ω^1 and Ω^2, with outward unit normal vectors $\boldsymbol{n}_1$ and $\boldsymbol{n}_2$, respectively, such that $\mathcal{I} := \overline{\Omega^1} \cap \overline{\Omega^2}$ represents the interface between the two subdomains. For $i \in \{1, 2\}$ and $h_i > 0$, let $\Omega^i_{h_i} = \{K\}$ denote a $(\Gamma \cap \partial\Omega^i)$-conforming triangulation of Ω^i, with boundary $\Gamma^i_{h_i}$, made of polyhedral elements K of size proportional to h_i. Without loss of generality, we suppose $h_2 \geq h_1$. We assume each element K is a simplex, a quadrilateral $(d = 2)$ or a hexahedron $(d = 3)$. Also, to simplify the notation, we will just write h instead of h_i when there is no confusion, i.e., when the label h indicates the size of the triangulation Ω^1_h or Ω^2_h. In this case, $\overline{\Omega^1_h} \cap \overline{\Omega^2_h}$ is not necessarily $\mathcal{I}$ as in the examples displayed in Figs 1 and 2. Then, for $i = 1, 2$ we define $\mathcal{I}^i_h := \Gamma^i_h \setminus \Gamma$ (see Fig. 3 for an illustration). The set of faces of the triangulation Ω^i_h will be denoted by $\mathcal{E}^i_h$.

The family of triangulations $\{\Omega^i_h\}_{h>0}$ is assumed to be shape-regular, i.e., there exists $\kappa_i > 0$ such that for all elements $K \in \Omega^i_h$ and all $h > 0$, $h_K/\rho_K \leq \kappa_i$, where h_K is the diameter of K and ρ_K is the diameter of the largest ball contained in K. For every element K, we will denote by $\boldsymbol{n}_K$ the outward unit

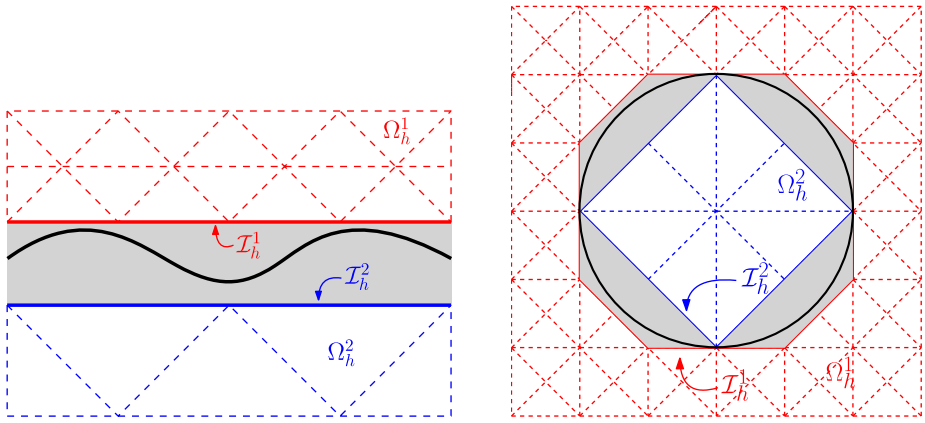

FIG. 3. Examples of computational domain and notation.

normal vector to K, writing $\boldsymbol{n}$ instead of $\boldsymbol{n}_K$ when there is no confusion. The set of all the faces e of Ω_h^i is denoted by $\mathcal{E}_h^i$.

Spaces and norms. Given an element K and a non-negative integer r, $\mathbb{P}_r(K)$ denotes the space of polynomials of total degree at most r on K and $\mathbb{Q}_r(K)$ the space of polynomials of degrees at most r for each variable on K. We also define $\mathbf{P}_r(K) := [\mathbb{P}_r(K)]^d$ and $\mathbf{Q}_r(K) := [\mathbb{Q}_r(K)]^d$. For any face e, $\mathbb{P}_r(e)$ denotes the space of polynomials of total degree at most r on e. Given a region $D \subset \mathbb{R}^d$, we denote by $(\cdot,\cdot)_D$ and $\langle\cdot,\cdot\rangle_{\partial D}$ the $L^2(D)$ and $L^2(\partial D)$ inner products, respectively. The L^2-norms over D and ∂D will be denoted by $\|\cdot\|_D$ and $\|\cdot\|_{\partial D}$. We use the standard notation for Sobolev spaces and their associated norms and seminorms, where vector-valued functions and their corresponding spaces are denoted in bold face.

For a given polynomial degree k, we introduce the finite-dimensional spaces

$$\begin{aligned}
\boldsymbol{V}_h^i &:= \{\boldsymbol{v} \in \boldsymbol{L}^2(\Omega_h^i) : \boldsymbol{v}|_K \in \boldsymbol{V}(K),\ \forall\, K \in \Omega_h^i\},\\
W_h^i &:= \{w \in L^2(\Omega_h^i) : w|_K \in W(K),\ \forall\, K \in \Omega_h^i\},\\
M_h^i &:= \{\mu \in L^2(\mathcal{E}_h^i) : \mu|_e \in M(e),\ \forall\, e \in \mathcal{E}_h^i\},\\
M_h(\mathcal{I}_h^i) &:= \{\mu \in L^2(\mathcal{I}_h^i) : \mu|_e \in M(e),\ \forall\, e \in \mathcal{I}_h^i\},
\end{aligned}$$

where $\boldsymbol{V}(K)$, $W(K)$ and $M(e)$ are local finite-dimensional spaces that can be defined in several ways (cf. Cockburn *et al.*, 2010). In particular, since we are considering simplices, quadrilaterals and hexahedra, we focus on the spaces specified in Table 1, where $\widetilde{P}_k(K)$ denotes the space of homogeneous polynomials of degree k defined on K.

The inner products for the triangulation Ω_h^i $(i = 1, 2)$ are given by

$$(\cdot,\cdot)_{\Omega_h^i} := \sum_{K\in\Omega_h^i} (\cdot,\cdot)_K, \qquad \langle\cdot,\cdot\rangle_{\partial\Omega_h^i} := \sum_{K\in\Omega_h^i} \langle\cdot,\cdot\rangle_{\partial K} \quad \text{and} \quad \langle\cdot,\cdot\rangle_{\mathcal{I}_h^i} := \sum_{e\in\mathcal{I}_h^i} \langle\cdot,\cdot\rangle_e,$$

TABLE 1 *Local finite-dimensional spaces for the HDG method for $k \geq 1$*

K	$V(K)$	$W(K)$	$M(e)$
Simplex	$\mathbf{P}_k(K)$	$\mathbb{P}_k(K)$	$\mathbb{P}_k(e)$
Square	$\mathbf{P}_k(K) \oplus \nabla \times (xy\widetilde{P}_k(K))$	$\mathbb{P}_k(K)$	$\mathbb{P}_k(e)$
Square	$\mathbf{Q}_k(K) \oplus \{(x^{k+1}, 0), (0, y^{k+1})\}$	$\mathbb{Q}_k(K)$	$\mathbb{Q}_k(e)$
Cube	$\mathbf{P}_k(K) \oplus \nabla \times (yz\widetilde{P}_k(K), 0, 0) \oplus \nabla \times (0, zx\widetilde{P}_k(K), 0)$	$\mathbb{P}_k(K)$	$\mathbb{P}_k(e)$

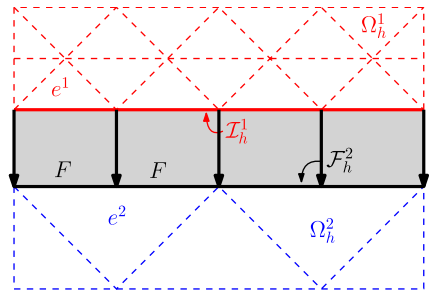

FIG. 4. $\mathcal{F}_h^2$ is the partition of $\mathcal{I}_h^2$ induced by $\mathcal{I}_h^1$. In this illustration, $e^2 \in \mathcal{I}_h^2$ is partitioned in two faces F.

and their corresponding norms will be denoted, respectively, by

$$\|\cdot\|_{\Omega_h^i} := \left(\sum_{K\in\Omega_h^i} \|\cdot\|_K^2\right)^{1/2}, \qquad \|\cdot\|_{\partial\Omega_h^i} := \left(\sum_{K\in\Omega_h^i} \|\cdot\|_{\partial K}^2\right)^{1/2} \quad \text{and} \quad \|\cdot\|_{\mathcal{I}_h^i} := \left(\sum_{e\in\mathcal{I}_h^i} \|\cdot\|_e^2\right)^{1/2}.$$

To avoid proliferation of unimportant constants, we will use the terminology $a \lesssim b$ whenever $a \leq Cb$ and C is a positive constant independent of h.

Connecting segments. We introduce a mapping $\boldsymbol{\phi} : \mathcal{I}_h^2 \to \mathcal{I}_h^1$, such that for each point $\boldsymbol{x}_2 \in \mathcal{I}_h^2$, we associate a point $\boldsymbol{x}_1 = \boldsymbol{\phi}(\boldsymbol{x}_2) \in \mathcal{I}_h^1$. We denote by $\sigma(\boldsymbol{x}_2)$ the segment starting at $\boldsymbol{x}_2$ and ending at $\boldsymbol{x}_1$, with unit tangent vector $\boldsymbol{m}$ and length $|\sigma(\boldsymbol{x}_2)|$. The segment $\sigma(\boldsymbol{x}_2)$ is referred as the *connecting segment* associated with $\boldsymbol{x}_2$ and is assumed to satisfy two conditions: it does not intersect the interior of another segment and its length $|\sigma(\boldsymbol{x}_2)|$ is of order at most $\max\{h_1, h_2\} = h_2$, where we recall that h_i is the meshsize of the triangulation Ω_h^i that satisfies $h_2 > h_1$.

Now, let $\boldsymbol{v}_2$ a vertex of $\mathcal{I}_h^2$. We assume that the point $\boldsymbol{v}_1$ associated with $\boldsymbol{v}_2$ is a vertex of $\mathcal{I}_h^1$. In Figs 2 and 3, this is always the case. Then, $\mathcal{I}_h^1$ induces a partition of $\mathcal{I}_h^2$ that we denoted by $\mathcal{F}_h^2 = \{F\}$. Figure 4 shows an illustration where the face e^1 induces a partition over the face e^2 such that $F = \boldsymbol{\phi}^{-1}(e^1)$. If that assumption holds, the numerical experiments may show orders of convergence higher than the error estimates (see Subsection 5.3). However, we think the error estimates are still valid if the assumption does not hold. For instance, the interfaces could be globally swapped, i.e., $\mathcal{I}_h^2$ could induce a partition on $\mathcal{I}_h^1$. Or the interfaces could be *locally* swapped, i.e., subsets of $\mathcal{I}_h^1$ and $\mathcal{I}_h^2$ would both induce partitions of their subsets complement on $\mathcal{I}_h^2$ and $\mathcal{I}_h^1$, respectively. The real requirement that needs to be satisfied

TABLE 2 *Local finite dimensional spaces for the HDG-projection*

K	$\widetilde{\boldsymbol{V}}(K)$	$\widetilde{W}(K)$
Simplex	$\mathbf{P}_{k-1}(K)$	$\mathbb{P}_{k-1}(K)$
Square	$\mathbf{P}_{k-1}(K)$	$\mathbb{P}_{k-1}(K)$
Square	$\nabla\mathbf{Q}_k(K) \oplus \mathbf{S}_k(K)$	$\mathbb{Q}_k(K) \setminus \{x^k y^k\}$
Cube	$\mathbf{P}_{k-1}(K)$	$\mathbb{P}_{k-1}(K)$

is that any face of one interface is mapped to a subset, of nonzero measure, of the other interface. This is to prevent a face from being associated with a single vertex.

Extrapolation operator. The region enclosed by Ω_h^1 and Ω_h^2 (shaded area in Figs 2 and 3) will be denoted by Ω_h^{ext}. We notice that Ω_h^{ext} is not meshed. As a consequence, we do not have an HDG approximation in there. That is why the HDG approximation of the flux $\boldsymbol{q}$ will be locally extrapolated from the computational domain $\Omega_h^1 \cup \Omega_h^2$ to Ω_h^{ext}. More precisely, let $\boldsymbol{p}|_K : \mathbf{P}_k(K) \to \mathbb{R}$ be a vector-valued polynomial function that is defined on an element K in $\Omega_h^1 \cup \Omega_h^2$ such that $\overline{K} \cap \overline{\Omega_h^{ext}} \neq \emptyset$. We will define its extension to Ω_h^{ext} as

$$\boldsymbol{E}_{\boldsymbol{p}|_K}(\boldsymbol{y}) := \boldsymbol{p}|_K(\boldsymbol{y}) \qquad \forall \boldsymbol{y} \in \Omega_h^{ext}. \tag{2.1}$$

Note that the extended function $\boldsymbol{E}_{\boldsymbol{p}|_K}(\boldsymbol{y})$ is a vector-valued polynomial function whose support includes Ω_h^{ext}. Each element K will have its own extended function.

The HDG-projection. In the analysis, we will employ the HDG projection devised in Cheung *et al.* (2019). More precisely, let τ be the stabilization parameter of the HDG method that we assume non-negative and uniformly bounded. For $i \in \{1, 2\}$ and a pair of functions $(\boldsymbol{q}^{(i)}, u^{(i)}) \in \boldsymbol{H}^1(\Omega_h^i) \times H^1(\Omega_h^i)$, we recall its HDG projection $\boldsymbol{\Pi}^i(\boldsymbol{q}^{(i)}, u^{(i)}) := (\boldsymbol{\Pi}_{\boldsymbol{V}^i}\boldsymbol{q}^{(i)}, \Pi_{W_i}u^{(i)}) \in \boldsymbol{V}_h^i \times W_h^i$ defined as the unique element-wise solution of

$$(\boldsymbol{\Pi}_{\boldsymbol{V}^i}\boldsymbol{q}^{(i)}, \boldsymbol{v})_K = (\boldsymbol{q}^{(i)}, \boldsymbol{v})_K \qquad \forall\, \boldsymbol{v} \in \widetilde{\mathbf{V}}(K), \tag{2.2a}$$

$$(\Pi_{W^i}u^{(i)}, w)_K = (u^{(i)}, w)_K \qquad \forall\, w \in \widetilde{W}(K), \tag{2.2b}$$

$$\langle \boldsymbol{\Pi}_{\boldsymbol{V}^i}\boldsymbol{q}^{(i)} \cdot \boldsymbol{n}_i + \tau \Pi_{W^i}u^{(i)}, \mu\rangle_e = \langle \boldsymbol{q}^{(i)} \cdot \boldsymbol{n}_i + \tau P_{M^i}u^{(i)}, \mu\rangle_e \qquad \forall\, \mu \in M(e), \forall\, e \subset \partial K, \tag{2.2c}$$

for every element $K \in \Omega_h^i$. Here, P_{M^i} is the L^2 projection into M_h^i, and the spaces $\widetilde{\mathbf{V}}(K)$ and $\widetilde{W}(K)$ are defined in Table 2 according to Cockburn *et al.* (2010), where $\mathbf{S}_k(K) := \{\boldsymbol{v} \in \mathbf{V}(K) : \nabla \cdot \boldsymbol{v} = 0$ and $\boldsymbol{v} \cdot n = 0$ on $\partial K\}$.

Given constants $l_{\boldsymbol{q}}$ and $l_u \in [0, k]$, if $(\boldsymbol{q}^{(i)}, u^{(i)}) \in \boldsymbol{H}^1(\Omega_h^i) \times H^1(\Omega_h^i) \in H^{l_{\boldsymbol{q}}+1}(\Omega_h^i) \times H^{l_u+1}(\Omega_h^i)$, by Cheung *et al.* (2019) and Cockburn *et al.* (2010),

$$\|\boldsymbol{\Pi}_{\boldsymbol{V}^i}\boldsymbol{q}^{(i)} - \boldsymbol{q}^{(i)}\|_K \lesssim h_K^{l_{\boldsymbol{q}}+1}|\boldsymbol{q}^{(i)}|_{\boldsymbol{H}^{l_{\boldsymbol{q}}+1}(K)} + h_K^{l_u+1}|u^{(i)}|_{H^{l_u+1}(K)}, \tag{2.3a}$$

$$\|\Pi_{W^i}u^{(i)} - u^{(i)}\|_K \lesssim h_K^{l_u+1}|u^{(i)}|_{H^{l_u+1}(K)} + h_K^{l_{\boldsymbol{q}}+1}|\nabla \cdot \boldsymbol{q}^{(i)}|_{H^{l_{\boldsymbol{q}}}(K)}, \tag{2.3b}$$

for all $K \in \Omega_h^i$.

Further notation and auxiliary estimates. Let $i \in \{1,2\}$. Given a face $e \in \mathcal{I}_h^i$ belonging to the element $K_e \in \Omega_h^i$, we define the *extrapolation patch* as

$$K_e^{ext} := \{\boldsymbol{x} + \boldsymbol{n}_i t : 0 \le t \le |\sigma(\boldsymbol{x})|, \boldsymbol{x} \in e\}. \tag{2.4}$$

We denote by $h_e^\perp$ (resp. δ_e) the largest distance of a point inside K_e^1 (resp. K_e^{ext}) to the plane determined by the face e. In other words,

$$h_e^\perp = \max_{\boldsymbol{x}\in K_e} |\mathrm{dist}(\boldsymbol{x}, e)|, \qquad \delta_e = \max_{\boldsymbol{x}\in e} |\sigma(\boldsymbol{x})|, \tag{2.5}$$

where $\mathrm{dist}(\boldsymbol{x}, e)$ denotes the distance from $\boldsymbol{x}$ to the face e. We note that, δ_e is a measure of the local size of the gap and $\delta := \max_e \delta_e$ is an upper bound of the size of the gap. We define the ratio $r_e := \delta_e / h_e^\perp$ and

$$R_i := \max_{e\in\mathcal{I}_h^i} r_e. \tag{2.6}$$

For $e \in \mathcal{I}_h^1 \cup \mathcal{I}_h^2$, we also define

$$\boldsymbol{\mathcal{V}}^k := \left\{\boldsymbol{p} \in \mathbf{V}(K_e^{ext}), \boldsymbol{p}\cdot\boldsymbol{n_e} \neq 0 \text{ on each } e \subset \partial K_e^{ext}\right\},$$

where we denoted by $\boldsymbol{n}_e$ the interior normal vector to K_e^{ext} along the face e, i.e., the exterior normal vector to K_e pointing in the direction of K_e^{ext}. We can then introduce the constants

$$C_e^{ext} := \frac{1}{\sqrt{r_e}} \sup_{\boldsymbol{\chi}\in\boldsymbol{\mathcal{V}}^k} \frac{\|\boldsymbol{\chi}\cdot\boldsymbol{n}_e\|_{K_e^{ext}}}{\|\boldsymbol{\chi}\cdot\boldsymbol{n}_e\|_{K_e}}, \qquad C_e^{inv} := h_e^\perp \sup_{\boldsymbol{\chi}\in\boldsymbol{\mathcal{V}}^k} \frac{\|\partial_{\boldsymbol{n}_e}\boldsymbol{\chi}\|_{K_e}}{\|\boldsymbol{\chi}\cdot\boldsymbol{n}_e\|_{K_e}}. \tag{2.7}$$

As proved in (Cockburn *et al.*, 2012, Lemma A.2), these constants are independent of the meshsize, but depend on the polynomial degree k. The superscripts in C_e^{inv} and C_e^{ext} refer to an inverse inequality constant and an extrapolation constant.

On the other hand, following the ideas in Cockburn *et al.* (2012), it is useful to introduce the following auxiliary functions. Let $e \in \mathcal{I}_h^2$ that belongs to K_e and K_e^{ext}. For a function $\boldsymbol{v}$, we define

$$\Lambda^{(i)}_{\boldsymbol{v}|_{K_e}}(\boldsymbol{x}_2) := \frac{1}{|\sigma(\boldsymbol{x}_2)|}\int_0^{|\sigma(\boldsymbol{x}_2)|} \left(\boldsymbol{v}|_{K_e}(\boldsymbol{x}_2 + \boldsymbol{n}_2 s) \boldsymbol{v}|_{K_e}(\boldsymbol{x}_i)\right)\cdot\boldsymbol{n}_2 \,\mathrm{d}s, \tag{2.8}$$

for $i = 1, 2$, where we recall that $\boldsymbol{x}_2 \in e$ and $\boldsymbol{x}_1 \in \mathcal{I}_h^1$ are connected by the segment $\sigma(\boldsymbol{x}_2)$. They satisfy (cf. Cockburn *et al.*, 2012, Lemma 5.2)

$$\||\sigma|^{1/2}\Lambda^{(i)}_{\boldsymbol{v}|_{K_e}}\|_e \le \frac{1}{\sqrt{3}} r_e^{3/2} C_e^{ext} C_e^{inv} \|\boldsymbol{v}\|_{K_e} \qquad \forall\, \boldsymbol{v} \in \boldsymbol{V}(K_e), \tag{2.9a}$$

$$\||\sigma|^{1/2}\Lambda^{(i)}_{\boldsymbol{v}|_{K_e}}\|_e \le \frac{1}{\sqrt{3}} r_e \|h_e^\perp \partial_n \boldsymbol{v}\cdot\boldsymbol{n}\|_{K_e^{ext}} \qquad \forall\, \boldsymbol{v} \in \boldsymbol{H}^1(K_e^{ext}). \tag{2.9b}$$

These estimates will be useful for our error analysis of the HDG method. Another important tool is based on Taylor series expansion of a function defined on $\mathcal{I}_h^2$ around a point $\mathcal{I}_h^1$. More precisely, the following result holds.

LEMMA 2.1 Suppose that $\boldsymbol{\phi} : \mathcal{I}_h^2 \to \mathcal{I}_h^1$ is a bijection. The following assertions hold true.

If $\psi \in H^2(\Omega)$ and $\boldsymbol{\varphi} := -\nabla\psi$ then

$$\||\sigma|^{-1/2}(\psi - \psi\circ\boldsymbol{\phi}) + |\sigma|^{1/2}(\boldsymbol{\varphi}\circ\boldsymbol{\phi})\cdot\boldsymbol{n}_2\|_{\mathcal{I}_h^2} \lesssim \delta\ \|\psi\|_{H^2(\Omega)}, \tag{2.10a}$$

$$\||\sigma|^{-1/2}(\psi - \psi\circ\boldsymbol{\phi})\|_{\mathcal{I}_h^2} \lesssim \delta^{1/2}\ \|\psi\|_{H^2(\Omega)}. \tag{2.10b}$$

If $\boldsymbol{\varphi} \in \boldsymbol{H}^1(\Omega)$ then

$$\||\sigma|^{-1/2}(\boldsymbol{\varphi} - \boldsymbol{\varphi}\circ\boldsymbol{\phi})\cdot\boldsymbol{n}_2\|_{\mathcal{I}_h^2} \lesssim |\boldsymbol{\varphi}|_{\boldsymbol{H}^1(\Omega)}. \tag{2.10c}$$

Let $F \in \mathcal{F}_h^2$, $e = \boldsymbol{\phi}(F) \in \mathcal{I}_h^1$ and K_e the element where e belongs. If $p \in \mathbb{P}_k(K_e)$ then

$$\|p - p\circ\boldsymbol{\phi}\|_F \lesssim C_e^{ext}\,\delta_e\ h_e^{-3/2}\,\|p\|_{K_e}. \tag{2.10d}$$

The proof of this lemma can be found in the appendix.

2.2 *The HDG method*

On each subdomain Ω_h^i, we seek an approximation $(\boldsymbol{q}_h^{(i)}, u_h^{(i)}, \widehat{u}_h^{(i)}) \in \boldsymbol{V}_h^i \times W_h^i \times M_h^i$ that satisfies

$$(\boldsymbol{q}_h^{(i)}, \boldsymbol{v})_{\Omega_h^i} - (u_h^{(i)}, \nabla\cdot\boldsymbol{v})_{\Omega_h^i} + \langle\widehat{u}_h^{(i)}, \boldsymbol{v}\cdot\boldsymbol{n}_i\rangle_{\partial\Omega_h^i} = 0, \tag{2.11a}$$

$$-(\boldsymbol{q}_h^{(i)}, \nabla w)_{\Omega_h^i} + \langle\widehat{\boldsymbol{q}}_h^{(i)}\cdot\boldsymbol{n}_i, w\rangle_{\partial\Omega_h^i} = (f, w)_{\Omega_h^i}, \tag{2.11b}$$

$$\langle\widehat{\boldsymbol{q}}_h^{(i)}\cdot\boldsymbol{n}_i, \mu\rangle_{\partial\Omega_h^i\setminus\Gamma_h^i} = 0, \tag{2.11c}$$

$$\langle\widehat{u}_h^{(i)}, \mu\rangle_{\Gamma_h^i\setminus\mathcal{I}_h^i} = 0, \tag{2.11d}$$

for all $(\boldsymbol{v}, w, \mu) \in \boldsymbol{V}_h^i \times W_h^i \times M_h^i$, where

$$\widehat{\boldsymbol{q}}_h^{(i)}\cdot\boldsymbol{n}_i := \boldsymbol{q}_h^{(i)}\cdot\boldsymbol{n}_i + \tau(u_h^{(i)} - \widehat{u}_h^{(i)}) \qquad \text{on} \qquad \partial\Omega_h^i \tag{2.11e}$$

and we recall that τ is a positive stabilization function defined in $\partial\Omega_h^1 \cup \partial\Omega_h^2$ assumed to be uniformly bounded. By simplicity of the exposition, we assume τ is constant everywhere. The above equations must be complemented with suitable transmission conditions across the interfaces $\mathcal{I}_h^1$ and $\mathcal{I}_h^2$ that we proceed to derive now.

In the general case, where the two meshes do not coincide, the interface $\mathcal{I}$ is somehow 'split' in two discrete interfaces, $\mathcal{I}_h^1$ and $\mathcal{I}_h^2$. Therefore, some transmission conditions have to be defined on both $\mathcal{I}_h^1$

and $\mathcal{I}_h^2$. For this study, we propose the following conditions:

$$\langle \widehat{u}_h^{(1)} - \widetilde{u}_h^{(2)}, \mu \rangle_{\mathcal{I}_h^1} = 0, \qquad \forall\, \mu \in M_h(\mathcal{I}_h^1), \tag{2.12a}$$

$$\langle \widehat{\boldsymbol{q}}_h^{(2)} \cdot \boldsymbol{n}_2 + \widetilde{q}_h^{(1)}, \mu \rangle_{\mathcal{I}_h^2} = 0, \qquad \forall\, \mu \in M_h(\mathcal{I}_h^2), \tag{2.12b}$$

where $\widetilde{u}_h^{(2)}$ and $\widetilde{q}_h^{(1)}$ are approximations of $u|_{\mathcal{I}_h^1}$ and $-\boldsymbol{q}\cdot\boldsymbol{n}_2|_{\mathcal{I}_h^2}$, resp., based on extensions of $\widehat{u}_h^{(2)}$ and $\boldsymbol{q}_h^{(1)}$, resp., outside their respective computational domains. The tilde variables are constructed as follows.

For $\widetilde{u}_h^{(2)}$, we employ the transferring technique in Cockburn *et al.* (2012, 2014): let $\boldsymbol{x}_2 \in \mathcal{I}_h^2$ and its corresponding point $\boldsymbol{x}_1 \in \mathcal{I}_h^1$. Integrating (1.1a) along the connecting segment $\sigma(\boldsymbol{x}_2)$, we obtain

$$u(\boldsymbol{x}_1) = u(\boldsymbol{x}_2) - |\sigma(\boldsymbol{x}_2)| \int_0^1 \boldsymbol{q}(\boldsymbol{x}(s)) \cdot \boldsymbol{m}(\boldsymbol{x}(s))\, \mathrm{d}s, \tag{2.13}$$

where $\boldsymbol{x}(s) = \boldsymbol{x}_2 + (\boldsymbol{x}_1 - \boldsymbol{x}_2)s$ and $s \in [0,1]$ is the parametrization of $\sigma(\boldsymbol{x}_2)$. Thus, motivated by this expression, we define

$$\widetilde{u}_h^{(2)}(\boldsymbol{x}_1) := \widehat{u}_h^{(2)}(\boldsymbol{x}_2) - |\sigma(\boldsymbol{x}_2)| \int_0^1 \boldsymbol{E}_{\boldsymbol{q}_h^{(2)}}(\boldsymbol{x}(s)) \cdot \boldsymbol{m}(\boldsymbol{x}(s))\, \mathrm{d}s. \tag{2.14a}$$

Here, $\boldsymbol{E}_{\boldsymbol{q}_h^{(2)}}(\boldsymbol{x})$ denotes the extension of $\boldsymbol{q}_h^{(2)}(\boldsymbol{x})$ outside the computational domain Ω_h^2 (cf. (2.1)). On the other hand, based on the form of the HDG numerical fluxes (2.11e), we define

$$\widetilde{q}_h^{(1)}(\boldsymbol{x}_2) := -\boldsymbol{E}_{\boldsymbol{q}_h^{(1)}}(\boldsymbol{x}_2) \cdot \boldsymbol{n}_2(\boldsymbol{x}_2) + \tau(u_h^{(1)}(\boldsymbol{x}_1) - \widehat{u}_h^{(1)}(\boldsymbol{x}_1)). \tag{2.14b}$$

Although it is not obvious, (2.14b) involves transfers of both $u_h^{(1)}$ and $\widehat{u}_h^{(1)}$ similar to (2.14a). However, as the same gradient $\boldsymbol{q}_h^{(1)}$ is used for both transfers, the integral terms cancel out and only the terms evaluated on $\boldsymbol{x}_1$ remain.

The first transmission condition (2.12a) can be regarded as a Dirichlet boundary condition imposed on subdomain Ω_h^1 by transferring Dirichlet data from $\mathcal{I}_h^2$ to $\mathcal{I}_h^1$ through the mapping in (2.14a). The second transmission condition (2.12b) imposes a Neumann boundary condition on subdomain Ω_h^2 by transferring fluxes from $\mathcal{I}_h^1$ to $\mathcal{I}_h^2$ through the mapping in (2.14b).

In the particular case of matching interfaces, namely $\overline{\Omega_h^1} \cap \overline{\Omega_h^2} = \mathcal{I} = \mathcal{I}_h^1 = \mathcal{I}_h^2$, the transmission conditions (2.12) becomes

$$\langle \widehat{u}_h^{(1)} - \widehat{u}_h^{(2)}, \mu \rangle_{\mathcal{I}} = 0, \qquad \forall\, \mu \in M_h(\mathcal{I}), \tag{2.15a}$$

$$\langle \widehat{\boldsymbol{q}}_h^{(2)} \cdot \boldsymbol{n}_2 + \widehat{\boldsymbol{q}}_h^{(1)} \cdot \boldsymbol{n}_1, \mu \rangle_{\mathcal{I}} = 0, \qquad \forall\, \mu \in M_h(\mathcal{I}), \tag{2.15b}$$

where $M_h(\mathcal{I}) = M_h(\mathcal{I}_h^1) = M_h(\mathcal{I}_h^2)$. The resulting HDG formulation is then similar to that of Huynh *et al.* (2013) without the interface source terms. It does not become exactly a regular HDG scheme since the trace is bi-valued at the interface $\mathcal{I}$. Nevertheless, the regular HDG solution would be recovered since the duplicated traces are equal thanks to (2.15a).

In summary, the HDG scheme (2.11) is now completely defined with the transmission conditions (2.12) and the extrapolation of the numerical trace/flux (2.14).

REMARK 2.2 Instead of the transmission conditions (2.12), it is also possible to alternatively choose

$$\langle \widehat{u}_h^{(2)} - \widetilde{u}_h^{(1)}, \mu \rangle_{\mathcal{I}_h^2} = 0, \qquad \forall\, \mu \in M_h(\mathcal{I}_h^2), \tag{2.16a}$$

$$\langle \widehat{\boldsymbol{q}}_h^{(1)} \cdot \boldsymbol{n}_1 + \widetilde{q}_h^{(2)}, \mu \rangle_{\mathcal{I}_h^1} = 0, \qquad \forall\, \mu \in M_h(\mathcal{I}_h^1), \tag{2.16b}$$

where, for $\boldsymbol{x}_1 \in \mathcal{I}_h^1$, its corresponding point $\boldsymbol{x}_2 \in \mathcal{I}_h^2$ and $\widetilde{\boldsymbol{x}}(s) = \boldsymbol{x}_2 + (\boldsymbol{x}_1 - \boldsymbol{x}_2)s$, for $s \in [0,1]$, we define

$$\widetilde{u}_h^{(1)}(\boldsymbol{x}_2) := \widehat{u}_h^{(2)}(\boldsymbol{x}_1) + |\sigma(\boldsymbol{x}_2)| \int_0^1 \boldsymbol{E}_{\boldsymbol{q}_h^{(1)}}(\widetilde{\boldsymbol{x}}(s)) \cdot \boldsymbol{m}(\widetilde{\boldsymbol{x}}(s))\, \mathrm{d}s, \tag{2.17a}$$

$$\widetilde{q}_h^{(2)}(\boldsymbol{x}_1) := -\boldsymbol{E}_{\boldsymbol{q}_h^{(2)}}(\boldsymbol{x}_1) \cdot \boldsymbol{n}_1(\boldsymbol{x}_2) + \tau(u_h^{(2)}(\boldsymbol{x}_2) - \widehat{u}_h^{(2)}(\boldsymbol{x}_2)). \tag{2.17b}$$

For the swapped transmission conditions (2.16), when there is no gap, but hanging nodes are present in $\mathcal{I} = \overline{\Omega_h^1} \cap \overline{\Omega_h^2}$, our method becomes very similar to the HDG method analyzed in de Boer *et al.* (2007) and Chen & Cockburn (2012) for semimatching meshes. Moreover, our numerical experiments, reported in Subsection 5.3, can achieve the orders of convergence predicted in Chen & Cockburn (2012). But even then, the two methods are not identical since the transmission condition (2.16) involves bi-valued traces at the interface $\mathcal{I}$. As a consequence, the order of convergence of the error in $\boldsymbol{q}$ guaranteed by the analysis will be of only $k + 1/2$, as will be explained in Remark 4.4.

3. Stability analysis

In this section, we will show, under certain assumptions, a stability estimate associated with (2.11) and (2.12). In order to use this estimate to obtain both, well-posedness and error bounds, we consider the same problem (2.11), but (2.11a) is replaced by

$$(\boldsymbol{q}_h^{(i)}, \boldsymbol{v})_{\Omega_h^i} - (u_h^{(i)}, \nabla \cdot \boldsymbol{v})_{\Omega_h^i} + \langle \widehat{u}_h^{(i)}, \boldsymbol{v} \cdot \boldsymbol{n}_i \rangle_{\partial\Omega_h^i} = (\boldsymbol{g}_i, \boldsymbol{v})_{\Omega_h^i}, \tag{3.1a}$$

where $\boldsymbol{g}_i \in L^2(\Omega_h^i)$ is a given function such that it is orthogonal to polynomials of degree $k-1$ and (2.12) is replaced by

$$\langle \widehat{u}_h^{(1)} - \widetilde{u}_h^{(2)}, \mu \rangle_{\mathcal{I}_h^1} = \langle f_1, \mu \rangle_{\mathcal{I}_h^1} \qquad \forall\, \mu \in M_h(\mathcal{I}_h^1), \tag{3.2a}$$

$$\langle \widehat{\boldsymbol{q}}_h^{(2)} \cdot \boldsymbol{n}_2 + \widetilde{q}_h^{(1)}, \mu \rangle_{\mathcal{I}_h^2} = \langle f_2, \mu \rangle_{\mathcal{I}_h^2} \qquad \forall\, \mu \in M_h(\mathcal{I}_h^2), \tag{3.2b}$$

where f_1 and f_2 are given functions in belonging to $L^2(\mathcal{I}_h^1)$ and $L^2(\mathcal{I}_h^2)$, respectively. In particular, to show well-posedness, $\boldsymbol{g}_i$ and f_i will be zero, whereas $\boldsymbol{g}_i$ and f_i will be related to projection errors when proving the error estimates.

For simplicity of exposition in the analysis, we assume that

(A.1) $\Omega_h^1 \cap \Omega_h^2 = \emptyset$, i.e., there is no overlap between the subdomains;

(A.2) the mapping $\boldsymbol{\phi} : \mathcal{I}_h^2 \to \mathcal{I}_h^1$ is a bijection;

(A.3) for each $e^1 \in \mathcal{I}_h^1$, $\boldsymbol{m} = \boldsymbol{n}_2$ and $\boldsymbol{m} = -\boldsymbol{n}_1$;

(A.4) $\delta\tau + \frac{1}{8}\max_{e\in\mathcal{I}_h^1}(C_e^{tr})^{-1}h_e^{1/2}\tau^{1/2} \leq \frac{1}{8}$;

(A.5) $\max_{e\in\mathcal{I}_h^1}\left(2\delta_e^{2/7} + \frac{1}{8}(C_e^{tr})^{-2}h_e\tau\right) \leq \frac{1}{4}$ and $\max_{e\in\mathcal{I}_h^2}\left(\delta_e\tau + 4^{-1}(C_e^{tr})^{-2}h_e\tau\right) \leq \frac{1}{4}$;

(A.6) $2C_1\max_{e\in\mathcal{I}_h^2}(\delta_e^{12/7}h_e^{-3}\tau^{-1} + \delta_e^2h_e^{-2}) + \frac{1}{3}\max_{e\in\mathcal{I}_h^2}\delta_e^3h_e^{-3}\kappa_2^3(C_e^{ext}C_e^{inv})^2 \leq \frac{1}{4}$, where C_1 is a positive constant, independent of the meshsize, which will appear in Lemma 3.5;

(A.7) $C_2C_{\delta,h}\max_{e\in\mathcal{I}_h^1}(\delta_e^{2/7}h_e^{-1}\tau)$ is small enough, where

$$C_{\delta,h} := C_1\left(\max_{e\in\mathcal{I}_h^2}(\delta_e^{5/7}\tau^{-1}) + \max_{e\in\mathcal{I}_h^2}\delta_e^2h_e^{-3}(C_e^{ext})^2 + \delta\tau + \delta + h^2\tau + h_1^{2\min\{1,k\}} + h_2^{2\min\{1,k\}}\right) \tag{3.3}$$

and C_2 is a positive constant, independent of the meshsize, which will appear in Lemma 3.6.

Assumptions (A.1) and (A.2) hold true, for instance, in the illustrations of Figs 2 and 3. Note that the purpose of (A.1) is to simplify the analysis, but our method still works, without any modification, when there are overlaps, as long as the other assumptions are satisfied (see the numerical results in Section 5). In theory, Assumption (A.2) is not a strong assumption when $\mathcal{I}_h^1$ and $\mathcal{I}_h^2$ share the same topological properties, which is expected when both meshes are built from the same CAD geometry. However, building the bijection $\boldsymbol{\phi}$ in three dimensions may be a difficult task in practice. These two assumptions will be assumed to hold along the manuscript without explicitly mentioning them.

Assumption (A.3) means that the direction of the connecting segments must be parallel to the normals computed at its ends. Combined with (A.2), it is a very strong assumption that rules out, for instance, any discontinuity of the normal $\boldsymbol{x}_2 \mapsto \boldsymbol{n}_2(\boldsymbol{x}_2)$ on surface $\mathcal{I}_h^2$. Such discontinuities appear in configurations depicted in Figs 2 and 3 (right). The choice of this strong assumption helps us to facilitate the presentation of the ideas behind the proofs. Fortunately, the estimates of this work are also true if, instead of (A.3), we assume $1 + \boldsymbol{m}\cdot\boldsymbol{n}_1$ and $1 - \boldsymbol{m}\cdot\boldsymbol{n}_2$ are small enough, i.e., the direction of the connecting segments does not deviate too much from the normals at its ends.

The reminder assumptions are smallness assumption that relate the meshsize and the size of the gap. Conditions and (A.4) and (A.5) are always satisfied for h small enough if $\delta \lesssim h$. To analyze the feasibility of the other assumptions, let us write $\delta = C_g h^{1+\gamma}$ with $C_g \geq 0$ and $\gamma > 0$ constants independent of the meshsize. Assumptions (A.6) and (A.7) are satisfied for all $\gamma \in (3/4, 1]$, if h is small enough. These are the strongest assumptions, since they indicate that our analysis holds if the gap size is at most of order $h^{7/4}$. However, our numerical experiments indicate that the method still works even if δ is of order h.

The main result of this section is the next stability estimate. For convenience of notation, we define

$$\begin{aligned}\|(\boldsymbol{q}_h, u_h, \widehat{u}_h, \widetilde{u}_h)\| := \Bigg(&\sum_{i=1}^{2}\|\boldsymbol{q}_h^{(i)}\|_{\Omega_h^i}^2 + \|\tau^{1/2}(u_h^{(i)} - \widehat{u}_h^{(i)})\|_{\partial\Omega_h^i}^2 \\ &+ \left\||\sigma|^{-1/2}\left(\widetilde{u}_h^{(2)}\circ\boldsymbol{\phi} - \widehat{u}_h^{(2)}\right)\right\|_{\mathcal{I}_h^2}^2 + \|\delta_e^{1/7}\tau^{1/2}\widehat{u}_h^{(1)}\|_{\mathcal{I}_h^1}^2\Bigg)^{1/2}.\end{aligned} \tag{3.4}$$

THEOREM 3.1 Suppose Assumptions A and elliptic regularity (cf. 3.12) hold true. If τ is of order one, $k \geq 1$ and $h < 1$ then there exists $h_0 \in (0,1)$, such that for all $h < h_0$, it holds

$$\|(\boldsymbol{q}_h, u_h, \widehat{u}_h, \widetilde{u}_h)\|^2 \lesssim |||f|||_\Omega^2 + \sum_{i=1}^{2} \|\boldsymbol{g}_i\|_{\Omega_h^i}^2 + \|h_e^{-1/2} P_{M^1} f_1\|_{\mathcal{I}_h^1}^2 + \|\delta_e^{1/7} P_{M^2} f_2\|_{\mathcal{I}_h^2}^2 \tag{3.5a}$$

and

$$\sum_{i=1}^{2} \|u_h^{(i)}\|_{\Omega_h^i}^2 \lesssim C_{\delta,h} \|(\boldsymbol{q}_h, u_h, \widehat{u}_h, \widetilde{u}_h)\|^2 + \sum_{i=1}^{2} \|P_{M^i} f_i\|_{\mathcal{I}_h^i}^2 + (h_1^2 + h_2^2)\|f\|_\Omega^2 + \sum_{i=1}^{2} h_i^2 \|\boldsymbol{g}_i\|_{\Omega_h^i}^2, \tag{3.5b}$$

where $C_{\delta,h}$ is the constant defined in (3.3).

COROLLARY 3.2 The HDG scheme (2.11) has a unique solution.

Proof. Let $i \in \{1,2\}$. We observe that $\boldsymbol{g}_i = 0$ and $f_i = 0$ in HDG scheme (2.11). Hence, if $f = 0$, by Theorem 3.1, $\boldsymbol{q}_h^{(i)} = \boldsymbol{0}$, $u_h^{(i)} = 0$, $\widehat{u}_h^{(i)} = 0$ and $\widetilde{u}_h^i = 0$. □

The proof of Theorem 3.1 is postponed to Section 3.3. To that end, we first provide two technical lemmas.

3.1 *An energy argument*

Before presenting the energy estimate, it is useful first to deduce how the transmission conditions (2.12) connect $\mathbb{T}^1 := \langle \widehat{\boldsymbol{q}}_h^{(1)} \cdot \boldsymbol{n}_1, \widehat{u}_h^{(1)} \rangle_{\mathcal{I}_h^1}$ and $\mathbb{T}^2 := \langle \widehat{\boldsymbol{q}}_h^{(2)} \cdot \boldsymbol{n}_2, \widehat{u}_h^{(2)} \rangle_{\mathcal{I}_h^2}$. To that end, we will decompose $\mathbb{T}_1 + \mathbb{T}_2$ in such a way that the mismatch between $\mathcal{I}_h^1$ and $\mathcal{I}_h^2$ is explicitly written in terms of $\widetilde{u}_h^{(2)} \circ \boldsymbol{\phi} - \widehat{u}_h^{(2)}$, and the difference between a polynomial and its extrapolation. In the particular case when $\mathcal{I}_h^1 = \mathcal{I}_h^2$, $\widetilde{u}_h^{(2)} = \widehat{u}_h^{(2)}$ and $\widehat{\boldsymbol{q}}_h^{(1)} \cdot \boldsymbol{n}_1 = \widetilde{q}_h^{(1)}$ and therefore $\mathbb{T}_1 + \mathbb{T}_2$ vanishes.

LEMMA 3.3 It holds that

$$\begin{aligned}
\mathbb{T}_1 + \mathbb{T}_2 = {} & \langle (\boldsymbol{E}_{\boldsymbol{q}_h^{(1)}} \cdot \boldsymbol{n}_2) \circ \boldsymbol{\phi}^{-1} + \boldsymbol{q}_h^{(1)} \cdot \boldsymbol{n}_1, \widehat{u}_h^{(1)} \rangle_{\mathcal{I}_h^1} + \left\| |\sigma|^{-1/2} \left(\widetilde{u}_h^{(2)} \circ \boldsymbol{\phi} - \widehat{u}_h^{(2)} \right) \right\|_{\mathcal{I}_h^2}^2 \\
& + \langle P_{M^1}((Id - P_{M^2})\widetilde{q}_h^{(1)} \circ \boldsymbol{\phi}^{-1}), \widetilde{u}_h^{(2)} \rangle_{\mathcal{I}_h^1} + \langle (Id - P_{M^1})((\widehat{\boldsymbol{q}}_h^{(2)} \cdot \boldsymbol{n}_2) \circ \boldsymbol{\phi}^{-1}), \widetilde{u}_h^{(2)} \rangle_{\mathcal{I}_h^1} \\
& + \langle \Lambda_{\boldsymbol{q}_h^{(2)}}^{(2)}, \widetilde{u}_h^{(2)} \circ \boldsymbol{\phi} - \widehat{u}_h^{(2)} \rangle_{\mathcal{I}_h^2} - \langle \tau(u_h^{(2)} - \widehat{u}_h^{(2)}), \widetilde{u}_h^{(2)} \circ \boldsymbol{\phi} - \widehat{u}_h^{(2)} \rangle_{\mathcal{I}_h^2} \\
& + \langle (Id - P_{M^2})\widetilde{q}_h^{(1)} + \widehat{\boldsymbol{q}}_h^{(2)} \cdot \boldsymbol{n}_2, (P_{M^1} f_1) \circ \boldsymbol{\phi} \rangle_{\mathcal{I}_h^2} + \langle (P_{M^2} f_2) \circ \boldsymbol{\phi}^{-1}, \widehat{u}_h^{(1)} \rangle_{\mathcal{I}_h^1} \\
& + \|\delta_e^{1/7} \tau^{1/2} \widehat{u}_h^{(1)}\|_{\mathcal{I}_h^1}^2 + \langle \delta_e^{2/7} \tau(u_h^{(1)} - \widehat{u}_h^{(1)}), \widehat{u}_h^{(1)} \rangle_{\mathcal{I}_h^1} - \langle \delta_e^{2/7} \tau u_h^{(1)}, \widehat{u}_h^{(1)} \rangle_{\mathcal{I}_h^1}.
\end{aligned}$$

Proof. We first add and subtract $\widetilde{u}_h^{(2)} \circ \boldsymbol{\phi}$ in the second argument of $\mathbb{T}_2$ and write

$$\mathbb{T}_2 = \langle \widehat{\boldsymbol{q}}_h^{(2)} \cdot \boldsymbol{n}_2, \widehat{u}_h^{(2)} - \widetilde{u}_h^{(2)} \circ \boldsymbol{\phi} \rangle_{\mathcal{I}_h^2} + \langle (\widehat{\boldsymbol{q}}_h^{(2)} \cdot \boldsymbol{n}_2) \circ \boldsymbol{\phi}, \widetilde{u}_h^{(2)} \rangle_{\mathcal{I}_h^1}.$$

We decompose the first argument of second term and use (3.2a) to rewrite

$$\begin{aligned}\mathbb{T}_2 = \langle \widehat{\boldsymbol{q}}_h^{(2)} \cdot \boldsymbol{n}_2, \widehat{u}_h^{(2)} - \widetilde{u}_h^{(2)} \circ \boldsymbol{\phi} \rangle_{\mathcal{I}_h^2} + \langle P_{M^1}((\widehat{\boldsymbol{q}}_h^{(2)} \cdot \boldsymbol{n}_2) \circ \boldsymbol{\phi}^{-1}), \widehat{u}_h^{(1)} \rangle_{\mathcal{I}_h^1} \\ + \langle P_{M^1}((\widehat{\boldsymbol{q}}_h^{(2)} \cdot \boldsymbol{n}_2) \circ \boldsymbol{\phi}^{-1}), f_1 \rangle_{\mathcal{I}_h^1} + \langle (Id - P_{M^1})((\widehat{\boldsymbol{q}}_h^{(2)} \cdot \boldsymbol{n}_2) \circ \boldsymbol{\phi}^{-1}), \widetilde{u}_h^{(2)} \rangle_{\mathcal{I}_h^1},\end{aligned}$$

where Id is the identity operator. Then,

$$\begin{aligned}\mathbb{T}_2 = \langle \widehat{\boldsymbol{q}}_h^{(2)} \cdot \boldsymbol{n}_2, \widehat{u}_h^{(2)} - \widetilde{u}_h^{(2)} \circ \boldsymbol{\phi} \rangle_{\mathcal{I}_h^2} + \langle \widehat{\boldsymbol{q}}_h^{(2)} \cdot \boldsymbol{n}_2, \widehat{u}_h^{(1)} \circ \boldsymbol{\phi} \rangle_{\mathcal{I}_h^2} \\ + \langle \widehat{\boldsymbol{q}}_h^{(2)} \cdot \boldsymbol{n}_2, (P_{M^1} f_1) \circ \boldsymbol{\phi} \rangle_{\mathcal{I}_h^2} + \langle (Id - P_{M^1})((\widehat{\boldsymbol{q}}_h^{(2)} \cdot \boldsymbol{n}_2) \circ \boldsymbol{\phi}^{-1}), \widetilde{u}_h^{(2)} \rangle_{\mathcal{I}_h^1}.\end{aligned}$$

On the other hand, we add and subtract $\widetilde{q}_h^{(1)} \circ \boldsymbol{\phi}^{-1}$ in the first argument of $\mathbb{T}_1$ and write

$$\mathbb{T}_1 = \langle \widehat{\boldsymbol{q}}_h^{(1)} \cdot \boldsymbol{n}_1 - \widetilde{q}_h^{(1)} \circ \boldsymbol{\phi}^{-1}, \widehat{u}_h^{(1)} \rangle_{\mathcal{I}_h^1} + \langle \widetilde{q}_h^{(1)} \circ \boldsymbol{\phi}^{-1}, \widehat{u}_h^{(1)} \rangle_{\mathcal{I}_h^1}.$$

We decompose the second argument of second term and use (3.2b) to rewrite

$$\begin{aligned}\mathbb{T}_1 = \langle \widehat{\boldsymbol{q}}_h^{(1)} \cdot \boldsymbol{n}_1 - \widetilde{q}_h^{(1)} \circ \boldsymbol{\phi}^{-1}, \widehat{u}_h^{(1)} \rangle_{\mathcal{I}_h^1} - \langle \widehat{\boldsymbol{q}}_h^{(2)} \cdot \boldsymbol{n}_2, P_{M^2}(\widehat{u}_h^{(1)} \circ \boldsymbol{\phi}) \rangle_{\mathcal{I}_h^2} \\ + \langle \widetilde{q}_h^{(1)}, (Id - P_{M^2})(\widehat{u}_h^{(1)} \circ \boldsymbol{\phi}) \rangle_{\mathcal{I}_h^2} + \langle f_2, P_{M^2}(\widehat{u}_h^{(1)} \circ \boldsymbol{\phi}) \rangle_{\mathcal{I}_h^2}.\end{aligned}$$

From (2.14b) and (2.11e), we have that

$$\widetilde{q}_h^{(1)} \circ \boldsymbol{\phi}^{-1} = -(\boldsymbol{E}_{\boldsymbol{q}_h^{(1)}} \cdot \boldsymbol{n}_2) \circ \boldsymbol{\phi}^{-1} - \boldsymbol{q}_h^{(1)} \cdot \boldsymbol{n}_1 + \widehat{\boldsymbol{q}}_h^{(1)} \cdot \boldsymbol{n}_1 \qquad \text{in} \qquad \mathcal{I}_h^1, \tag{3.6}$$

which implies that

$$\begin{aligned}\mathbb{T}_1 = \langle (\boldsymbol{E}_{\boldsymbol{q}_h^{(1)}} \cdot \boldsymbol{n}_2) \circ \boldsymbol{\phi}^{-1} + \boldsymbol{q}_h^{(1)} \cdot \boldsymbol{n}_1, \widehat{u}_h^{(1)} \rangle_{\mathcal{I}_h^1} - \langle \widehat{\boldsymbol{q}}_h^{(2)} \cdot \boldsymbol{n}_2, \widehat{u}_h^{(1)} \circ \boldsymbol{\phi} \rangle_{\mathcal{I}_h^2} \\ + \langle \widetilde{q}_h^{(1)}, (Id - P_{M^2})(\widehat{u}_h^{(1)} \circ \boldsymbol{\phi}) \rangle_{\mathcal{I}_h^2} + \langle (P_{M^2} f_2) \circ \boldsymbol{\phi}^{-1}, \widehat{u}_h^{(1)} \rangle_{\mathcal{I}_h^1}.\end{aligned}$$

Moreover, by (3.2a), the third term becomes

$$\begin{aligned}\langle ((Id - P_{M^2})\widetilde{q}_h^{(1)}) \circ \boldsymbol{\phi}^{-1}, \widehat{u}_h^{(1)} \rangle_{\mathcal{I}_h^1} \\ = \langle P_{M^1}((Id - P_{M^2})\widetilde{q}_h^{(1)} \circ \boldsymbol{\phi}^{-1}), \widetilde{u}_h^{(2)} \rangle_{\mathcal{I}_h^1} + \langle P_{M^1}((Id - P_{M^2})\widetilde{q}_h^{(1)} \circ \boldsymbol{\phi}^{-1}), f_1 \rangle_{\mathcal{I}_h^1}.\end{aligned}$$

Thus, we obtain

$$\begin{aligned}\mathbb{T}_1+\mathbb{T}_2 &= \langle (\boldsymbol{E}_{\boldsymbol{q}_h^{(1)}}\cdot\boldsymbol{n}_2)\circ\boldsymbol{\phi}^{-1}+\boldsymbol{q}_h^{(1)}\cdot\boldsymbol{n}_1,\widehat{u}_h^{(1)}\rangle_{\mathcal{I}_h^1}+\langle\widehat{\boldsymbol{q}}_h^{(2)}\cdot\boldsymbol{n}_2,\widehat{u}_h^{(2)}-\widetilde{u}_h^{(2)}\circ\boldsymbol{\phi}\rangle_{\mathcal{I}_h^2}\\ &\quad+\langle P_{M^1}((Id-P_{M^2})\widetilde{q}_h^{(1)}\circ\boldsymbol{\phi}^{-1}),\widetilde{u}_h^{(2)}\rangle_{\mathcal{I}_h^1}+\langle(Id-P_{M^1})((\widehat{\boldsymbol{q}}_h^{(2)}\cdot\boldsymbol{n}_2)\circ\boldsymbol{\phi}^{-1}),\widetilde{u}_h^{(2)}\rangle_{\mathcal{I}_h^1}\\ &\quad+\langle(Id-P_{M^2})\widetilde{q}_h^{(1)}+\widehat{\boldsymbol{q}}_h^{(2)}\cdot\boldsymbol{n}_2,(P_{M^1}f_1)\circ\boldsymbol{\phi}\rangle_{\mathcal{I}_h^2}+\langle(P_{M^2}f_2)\circ\boldsymbol{\phi}^{-1},\widehat{u}_h^{(1)}\rangle_{\mathcal{I}_h^1}.\end{aligned}$$

For convenience, in order to have the term $\|\delta_e^{1/7}\tau^{1/2}\widehat{u}_h^{(1)}\|^2_{\mathcal{I}_h^1}$ on the left-hand side of the stability estimate, we add $0=\langle\delta_e^{2/7}\tau\widehat{u}_h^{(1)},\widehat{u}_h^{(1)}\rangle_{\mathcal{I}_h^1}+\langle\delta_e^{2/7}\tau(u_h^{(1)}-\widehat{u}_h^{(1)}),\widehat{u}_h^{(1)}\rangle_{\mathcal{I}_h^1}-\langle\delta_e^{2/7}\tau u_h^{(1)},\widehat{u}_h^{(1)}\rangle_{\mathcal{I}_h^1}$. Then,

$$\begin{aligned}\mathbb{T}_1+\mathbb{T}_2 &= \langle (\boldsymbol{E}_{\boldsymbol{q}_h^{(1)}}\cdot\boldsymbol{n}_2)\circ\boldsymbol{\phi}^{-1}+\boldsymbol{q}_h^{(1)}\cdot\boldsymbol{n}_1,\widehat{u}_h^{(1)}\rangle_{\mathcal{I}_h^1}+\langle\widehat{\boldsymbol{q}}_h^{(2)}\cdot\boldsymbol{n}_2,\widehat{u}_h^{(2)}-\widetilde{u}_h^{(2)}\circ\boldsymbol{\phi}\rangle_{\mathcal{I}_h^2}\\ &\quad+\langle P_{M^1}((Id-P_{M^2})\widetilde{q}_h^{(1)}\circ\boldsymbol{\phi}^{-1}),\widetilde{u}_h^{(2)}\rangle_{\mathcal{I}_h^1}+\langle(Id-P_{M^1})((\widehat{\boldsymbol{q}}_h^{(2)}\cdot\boldsymbol{n}_2)\circ\boldsymbol{\phi}^{-1}),\widetilde{u}_h^{(2)}\rangle_{\mathcal{I}_h^1}\\ &\quad+\langle(Id-P_{M^2})\widetilde{q}_h^{(1)}+\widehat{\boldsymbol{q}}_h^{(2)}\cdot\boldsymbol{n}_2,(P_{M^1}f_1)\circ\boldsymbol{\phi}\rangle_{\mathcal{I}_h^2}+\langle(P_{M^2}f_2)\circ\boldsymbol{\phi}^{-1},\widehat{u}_h^{(1)}\rangle_{\mathcal{I}_h^1}\\ &\quad+\|\delta_e^{1/7}\,\tau^{1/2}\widehat{u}_h^{(1)}\|^2_{\mathcal{I}_h^1}+\langle\delta_e^{2/7}\tau(u_h^{(1)}-\widehat{u}_h^{(1)}),\widehat{u}_h^{(1)}\rangle_{\mathcal{I}_h^1}-\langle\delta_e^{2/7}\,\tau u_h^{(1)},\widehat{u}_h^{(1)}\rangle_{\mathcal{I}_h^1}.\end{aligned}$$

From now on, we will abusively denote $\boldsymbol{n}_1(\boldsymbol{x}_2)$ instead of $\boldsymbol{n}_1\circ\boldsymbol{\phi}(\boldsymbol{x}_2)$ for any $\boldsymbol{x}_2\in\mathcal{I}_h^2$.

On the other hand, since by assumption (A.2) $\boldsymbol{m}(\boldsymbol{x}(s))=\boldsymbol{n}_2$ for all $s\in[0,1]$, then $\boldsymbol{x}(s)=\boldsymbol{x}_2+(\boldsymbol{x}_1-\boldsymbol{x}_2)s=\boldsymbol{x}_2+\boldsymbol{n}_2|\sigma(\boldsymbol{x}_2)|s$ and (2.14a) can be rewritten as

$$\begin{aligned}\widetilde{u}_h^{(2)}(\boldsymbol{x}_1) &= \widehat{u}_h^{(2)}(\boldsymbol{x}_2)-\int_0^{|\sigma(\boldsymbol{x}_2)|}\boldsymbol{E}_{\boldsymbol{q}_h^{(2)}}(\boldsymbol{x}_2+\boldsymbol{n}_2 s)\cdot\boldsymbol{n}_2\,\mathrm{d}s\\ &= \widehat{u}_h^{(2)}(\boldsymbol{x}_2)-\int_0^{|\sigma(\boldsymbol{x}_2)|}\left(\boldsymbol{E}_{\boldsymbol{q}_h^{(2)}}(\boldsymbol{x}_2+\boldsymbol{n}_2 s)\cdot\boldsymbol{n}_2-\boldsymbol{q}_h^{(2)}(\boldsymbol{x}_2)\cdot\boldsymbol{n}_2\right)\mathrm{d}s-|\sigma(\boldsymbol{x}_2)|\boldsymbol{q}_h^{(2)}(\boldsymbol{x}_2)\cdot\boldsymbol{n}_2\\ &= \widehat{u}_h^{(2)}(\boldsymbol{x}_2)-|\sigma(\boldsymbol{x}_2)|\Lambda^{(2)}_{\boldsymbol{q}_h^{(2)}}(\boldsymbol{x}_2)-|\sigma(\boldsymbol{x}_2)|\boldsymbol{q}_h^{(2)}(\boldsymbol{x}_2)\cdot\boldsymbol{n}_2,\end{aligned}$$

where we used the definition in (2.8). This implies that

$$\boldsymbol{q}_h^{(2)}(\boldsymbol{x}_2)\cdot\boldsymbol{n}_2=-|\sigma(\boldsymbol{x}_2)|^{-1}(\widetilde{u}_h^{(2)}(\boldsymbol{x}_1)-\widehat{u}_h^{(2)}(\boldsymbol{x}_2))-\Lambda^{(2)}_{\boldsymbol{q}_h^{(2)}}(\boldsymbol{x}_2). \tag{3.7}$$

The result follows from the above expression for $\mathbb{T}_1+\mathbb{T}_2$ and (3.7). □

COROLLARY 3.4 If Assumption (A.3) holds then

$$\begin{aligned}\mathbb{T}_1+\mathbb{T}_2 &= \langle (\boldsymbol{E}_{\boldsymbol{q}_h^{(1)}}\cdot\boldsymbol{n}_2)\circ\boldsymbol{\phi}^{-1}+\boldsymbol{q}_h^{(1)}\cdot\boldsymbol{n}_1,\widehat{u}_h^{(1)}\rangle_{\mathcal{I}_h^1}+\left\||\sigma|^{-1/2}\left(\widetilde{u}_h^{(2)}\circ\boldsymbol{\phi}-\widehat{u}_h^{(2)}\right)\right\|^2_{\mathcal{I}_h^2}\\ &+\langle\Lambda^{(2)}_{\boldsymbol{q}_h^{(2)}},\widetilde{u}_h^{(2)}\circ\boldsymbol{\phi}-\widehat{u}_h^{(2)}\rangle_{\mathcal{I}_h^2}-\langle\tau(u_h^{(2)}-\widehat{u}_h^{(2)}),\widetilde{u}_h^{(2)}\circ\boldsymbol{\phi}-\widehat{u}_h^{(2)}\rangle_{\mathcal{I}_h^2}\\ &+\|\delta_e^{1/7}\tau^{1/2}\widehat{u}_h^{(1)}\|^2_{\mathcal{I}_h^1}+\langle\delta_e^{2/7}\tau(u_h^{(1)}-\widehat{u}_h^{(1)}),\widehat{u}_h^{(1)}\rangle_{\mathcal{I}_h^1}-\langle\delta_e^{2/7}\tau u_h^{(1)},\widehat{u}_h^{(1)}\rangle_{\mathcal{I}_h^1}\\ &+\langle(Id-P_{M^2})\widetilde{q}_h^{(1)}+\widehat{\boldsymbol{q}}_h^{(2)}\cdot\boldsymbol{n}_2,(P_{M^1}f_1)\circ\boldsymbol{\phi}\rangle_{\mathcal{I}_h^2}+\langle(P_{M^2}f_2)\circ\boldsymbol{\phi}^{-1},\widehat{u}_h^{(1)}\rangle_{\mathcal{I}_h^1}.\end{aligned}$$

Proof. By Assumption (A.3), $\boldsymbol{\phi}$ is a piecewise affine mapping and then $p\circ\boldsymbol{\phi}^{-1}\in M_h^1$ for all $p\in M_h^2$. Thus, the fourth term in the identity of previous lemma vanishes. Moreover, we notice that under Assumption (A.3), $P_{M^1}\widetilde{u}_h^{(2)}=\widetilde{u}_h^{(2)}$ and $\widetilde{u}_h^{(2)}\circ\boldsymbol{\phi}$ is a polynomial of degree k on every face of $\mathcal{I}_h^2$; hence, the third term also vanishes. □

We now employ an energy argument to obtain a bound for the L^2-norm of the approximation of the flux $\boldsymbol{q}_h^{(i)}$, the L^2-norm of the consistency error in the stabilization term $\tau^{1/2}(u_h^{(i)}-\widehat{u}_h^{(i)})$ and also the L^2-norm of the term $|\sigma|^{-1/2}\left(\widetilde{u}_h^{(2)}\circ\boldsymbol{\phi}-\widehat{u}_h^{(2)}\right)$ that indicates the error associated with the transferred transmission condition of the scalar variable. As we will see, the right-hand side of this bound depends, in addition to the sources, on terms involving the extrapolated polynomials and also on the L^2-norm of the approximation of u.

LEMMA 3.5 If Assumption (A) holds then there exists a constant $C_1>0$, independent of the meshsize, such that

$$\begin{aligned}\|(\boldsymbol{q}_h,u_h,\widehat{u}_h,\widetilde{u}_h)\|^2\le 8C_1\Bigg(&\|f\|^2_\Omega+\sum_{i=1}^2\|\boldsymbol{g}_i\|^2_{\Omega_h^i}+\sum_{i=1}^2\|u_h^{(i)}\|^2_{\Omega_h^i}\\ &\max_{e\in\mathcal{I}_h^1}(\delta_e^{2/7}C_{tr}^e h_e^{-1}\tau)\|u_h^{(1)}\|^2_{\Omega_h^1}+\|h_e^{-1/2}P_{M^1}f_1\|^2_{\mathcal{I}_h^1}+\|\delta_e^{1/7}\tau^{-1/2}P_{M^2}f_2\|^2_{\mathcal{I}_h^2}\Bigg).\end{aligned}\tag{3.8}$$

Proof. First of all, by testing equations (3.1a) and (2.11b)–(2.11d) with

$$\boldsymbol{v}=\begin{cases}\boldsymbol{q}_h^{(1)} & \text{in}\quad \Omega_h^1\\ \boldsymbol{q}_h^{(2)} & \text{in}\quad \Omega_h^2\end{cases},\quad w=\begin{cases}u_h^{(1)} & \text{in}\quad \Omega_h^1\\ u_h^{(2)} & \text{in}\quad \Omega_h^2\end{cases}\text{ and }\mu=\begin{cases}\widehat{u}_h^{(1)} & \text{in}\quad \partial\Omega_h^1\setminus\Gamma_h^1\\ \widehat{u}_h^{(2)} & \text{in}\quad \partial\Omega_h^2\setminus\Gamma_h^2\\ \widehat{\boldsymbol{q}}_h^{(1)}\cdot\boldsymbol{n}_1 & \text{in}\quad \Gamma_h^1\setminus\mathcal{I}_h^1\\ \widehat{\boldsymbol{q}}_h^{(2)}\cdot\boldsymbol{n}_2 & \text{in}\quad \Gamma_h^2\setminus\mathcal{I}_h^2\end{cases},$$

and adding them up, we obtain

$$\sum_{i=1}^2\|\boldsymbol{q}_h^{(i)}\|^2_{\Omega_h^i}+\|\tau^{1/2}(u_h^{(i)}-\widehat{u}_h^{(i)})\|^2_{\partial\Omega_h^i}+\mathbb{T}^i=\sum_{i=1}^2(f,u_h^{(i)})_{\Omega_h^i}+\sum_{i=1}^2(\boldsymbol{g}_i,\boldsymbol{q}_h^{(i)})_{\Omega_h^i}.\tag{3.9}$$

Combining this identity with the expression for $\mathbb{T}_1 + \mathbb{T}_2$ in Corollary 3.4 and recalling (3.4), we obtain

$$\|(\boldsymbol{q}_h, u_h, \widehat{u}_h, \widetilde{u}_h)\|^2 = \sum_{i=1}^{8} I_i + \sum_{i=1}^{2} (f, u_h^{(i)})_{\Omega_h^i} + \sum_{i=1}^{2} (\boldsymbol{g}_i, \boldsymbol{q}_h^{(i)})_{\Omega_h^i},$$

where

$$\begin{aligned}
I_1 &:= -\langle (\boldsymbol{E}_{\boldsymbol{q}_h^{(1)}} \cdot \boldsymbol{n}_2) \circ \boldsymbol{\phi}^{-1} + \boldsymbol{q}_h^{(1)} \cdot \boldsymbol{n}_1, \widehat{u}_h^{(1)} \rangle_{\mathcal{I}_h^1}, & I_2 &:= -\langle \Lambda^{(2)}_{\boldsymbol{q}_h^{(2)}}, \widetilde{u}_h^{(2)} \circ \boldsymbol{\phi} - \widehat{u}_h^{(2)} \rangle_{\mathcal{I}_h^2}, \\
I_3 &:= \langle \tau (u_h^{(2)} - \widehat{u}_h^{(2)}), \widetilde{u}_h^{(2)} \circ \boldsymbol{\phi} - \widehat{u}_h^{(2)} \rangle_{\mathcal{I}_h^2}, & I_4 &:= -\langle \delta_e^{2/7} \tau (u_h^{(1)} - \widehat{u}_h^{(1)}), \widehat{u}_h^{(1)} \rangle_{\mathcal{I}_h^1}, \\
I_5 &:= \langle \delta_e^{2/7} \tau u_h^{(1)}, \widehat{u}_h^{(1)} \rangle_{\mathcal{I}_h^1}, & I_6 &:= -\langle (P_{M^2} f_2) \circ \boldsymbol{\phi}^{-1}, \widehat{u}_h^{(1)} \rangle_{\mathcal{I}_h^1}, \\
I_7 &:= -\langle (Id - P_{M^2}) \widetilde{q}_h^{(1)}, (P_{M^1} f_1) \circ \boldsymbol{\phi} \rangle_{\mathcal{I}_h^2}, & I_8 &:= -\langle \widehat{\boldsymbol{q}}_h^{(2)} \cdot \boldsymbol{n}_2, (P_{M^1} f_1) \circ \boldsymbol{\phi} \rangle_{\mathcal{I}_h^2}.
\end{aligned}$$

Now, by Young's inequality, we bound each of these terms as follows. First,

$$I_1 \leq 2\|\delta_e^{-1/7} \tau^{-1/2} (\boldsymbol{E}_{\boldsymbol{q}_h^{(1)}} - \boldsymbol{q}_h^{(1)} \circ \boldsymbol{\phi})\|^2_{\mathcal{I}_h^2} + \frac{1}{8} \|\delta_e^{1/7} \tau^{1/2} \widehat{u}_h^{(1)}\|^2_{\mathcal{I}_h^1},$$

where we have used Assumptions (A.2) and (A.3). For I_2, we consider the estimate (2.9a) and the fact that $r_e \leq \delta_e h_e^{-1} \kappa_2$, where we recall that κ_2 is the mesh regularity constant of Ω_h^2, to obtain

$$\begin{aligned}
I_2 &\leq \||\sigma|^{1/2} \Lambda^{(2)}_{\boldsymbol{q}_h^{(2)}}\|^2_{\mathcal{I}_h^2} + \frac{1}{4} \||\sigma|^{-1/2} (\widetilde{u}_h^{(2)} \circ \boldsymbol{\phi} - \widehat{u}_h^{(2)})\|^2_{\mathcal{I}_h^2} \\
&\leq \frac{1}{3} \max_{e \in \mathcal{I}_h^2} (\delta_e^3 h_e^{-3} \kappa_2^3 (C_{ext}^2 C_{inv}^e)^2) \|\boldsymbol{q}_h^{(2)}\|^2_{\Omega_h^2} + \frac{1}{4} \||\sigma|^{-1/2} (\widetilde{u}_h^{(2)} \circ \boldsymbol{\phi} - \widehat{u}_h^{(2)})\|^2_{\mathcal{I}_h^2} \\
&\leq \frac{1}{4} \|\boldsymbol{q}_h^{(2)}\|^2_{\Omega_h^2} + \frac{1}{4} \||\sigma|^{-1/2} (\widetilde{u}_h^{(2)} \circ \boldsymbol{\phi} - \widehat{u}_h^{(2)})\|^2_{\mathcal{I}_h^2},
\end{aligned}$$

where we used Assumption (A.5). For I_3 and I_4, we consider Assumption (A.4), to obtain that

$$\begin{aligned}
I_3 &\leq \||\sigma|^{1/2} \tau (u_h^{(2)} - \widehat{u}_h^{(2)})\|^2_{\mathcal{I}_h^2} + \frac{1}{4} \||\sigma|^{-1/2} (\widetilde{u}_h^{(2)} \circ \boldsymbol{\phi} - \widehat{u}_h^{(2)})\|^2_{\mathcal{I}_h^2} \\
&\leq \frac{1}{4} \|\tau^{1/2} (u_h^{(2)} - \widehat{u}_h^{(2)})\|^2_{\mathcal{I}_h^2} + \frac{1}{4} \||\sigma|^{-1/2} (\widetilde{u}_h^{(2)} \circ \boldsymbol{\phi} - \widehat{u}_h^{(2)})\|^2_{\mathcal{I}_h^2},
\end{aligned}$$

and

$$\begin{aligned}
I_4 &\leq 2\|\delta_e^{1/7} \tau^{1/2} (u_h^{(1)} - \widehat{u}_h^{(1)})\|^2_{\mathcal{I}_h^1} + \frac{1}{8} \|\delta_e^{1/7} \tau^{1/2} \widehat{u}_h^{(1)}\|^2_{\mathcal{I}_h^1} \\
&\leq \frac{1}{4} \|\tau^{1/2} (u_h^{(1)} - \widehat{u}_h^{(1)})\|^2_{\mathcal{I}_h^1} + \frac{1}{8} \|\delta_e^{1/7} \tau^{1/2} \widehat{u}_h^{(1)}\|^2_{\mathcal{I}_h^1}.
\end{aligned}$$

For I_5, we have

$$I_5 \leq 2\|\delta_e^{1/7}\tau^{1/2}u_h^{(1)}\|^2_{\mathcal{I}_h^1} + \frac{1}{8}\|\delta_e^{1/7}\tau^{1/2}\widehat{u}_h^{(1)}\|^2_{\mathcal{I}_h^1},$$

and, for I_6,

$$I_6 \leq 2\|\delta_e^{-1/7}\tau^{-1/2}P_{M^2}f_2\|^2_{\mathcal{I}_h^2} + \frac{1}{8}\|\delta_e^{1/7}\tau^{1/2}\widehat{u}_h^{(1)}\|^2_{\mathcal{I}_h^1}.$$

For I_7, we use the definition of $\widetilde{q}_h^{(1)}$ in (2.14b), add and subtract $\boldsymbol{q}_h^{(1)} \circ \boldsymbol{\phi}$ and consider the discrete trace, inequality with constant $C_{tr}^e > 0$ independent of the meshsize, to obtain that

$$\begin{aligned}
I_7 &\leq 6\|C_e^{tr}h_e^{-1/2}P_{M^1}f_1\|^2_{\mathcal{I}_h^1} + \frac{1}{24}\|(C_e^{tr})^{-1}h_e^{1/2}\widetilde{q}_h^{(1)} \circ \boldsymbol{\phi}^{-1}\|^2_{\mathcal{I}_h^1} \\
&\leq 6\|C_e^{tr}h_e^{-1/2}P_{M^1}f_1\|^2_{\mathcal{I}_h^1} + \frac{1}{8}\left(\|(C_e^{tr})^{-1}h_e^{1/2}(\boldsymbol{E}_{\boldsymbol{q}_h^{(1)}} - \boldsymbol{q}_h^{(1)} \circ \boldsymbol{\phi})\|^2_{\mathcal{I}_h^2} + \|\boldsymbol{q}_h^{(1)}\|^2_{\Omega_h^1} + \|(C_e^{tr})^{-1}h_e^{1/2}\tau(u_h^{(1)} - \widehat{u}_h^{(1)})\|^2_{\mathcal{I}_h^1}\right) \\
&\leq 6\|C_e^{tr}h_e^{-1/2}P_{M^1}f_1\|^2_{\mathcal{I}_h^1} + \frac{1}{8}\|(C_e^{tr})^{-1}h_e^{1/2}(\boldsymbol{E}_{\boldsymbol{q}_h^{(1)}} - \boldsymbol{q}_h^{(1)} \circ \boldsymbol{\phi})\|^2_{\mathcal{I}_h^2} + \frac{1}{8}\|\boldsymbol{q}_h^{(1)}\|^2_{\Omega_h^1} + \frac{1}{4}\|\tau^{1/2}(u_h^{(1)} - \widehat{u}_h^{(1)})\|^2_{\mathcal{I}_h^1},
\end{aligned}$$

where we used Assumption (A.4) in the last inequality. A similar argument, but using the definition of $\widehat{\boldsymbol{q}}_h^{(2)} \cdot \boldsymbol{n}_2$ in (2.11e), yields

$$\begin{aligned}
I_8 &\leq 2\|C_e^{tr}h_e^{-1/2}P_{M^1}f_1\|^2_{\mathcal{I}_h^1} + \frac{1}{8}\|(C_e^{tr})^{-1}h_e^{1/2}\,(\widehat{\boldsymbol{q}}_h^{(2)} \cdot \boldsymbol{n}_2) \circ \boldsymbol{\phi}^{-1}\|^2_{\mathcal{I}_h^1} \\
&\leq 2\|C_e^{tr}h_e^{-1/2}P_{M^1}f_1\|^2_{\mathcal{I}_h^1} + \frac{1}{4}\left(\|\boldsymbol{q}_h^{(2)}\|^2_{\Omega_h^2} + \|(C_e^{tr})^{-1}h_e^{1/2}\tau(u_h^{(2)} - \widehat{u}_h^{(2)})\|^2_{\mathcal{I}_h^2}\right) \\
&\leq 2\|C_e^{tr}h_e^{-1/2}P_{M^1}f_1\|^2_{\mathcal{I}_h^1} + \frac{1}{4}\|\boldsymbol{q}_h^{(2)}\|^2_{\Omega_h^2} + \frac{1}{4}\|\tau^2(u_h^{(2)} - \widehat{u}_h^{(2)})\|^2_{\mathcal{I}_h^2}.
\end{aligned}$$

Thus, by Definition 3.4 and rearranging terms, we obtain

$$\begin{aligned}
\frac{1}{4}\|(\boldsymbol{q}_h, u_h, \widehat{u}_h, \widetilde{u}_h)\|^2 \leq\ & 2\|(\delta_e^{-1/7}\tau^{-1/2} + 4^{-1}(C_e^{tr})^{-1}h_e^{1/2})(\boldsymbol{E}_{\boldsymbol{q}_h^{(1)}} - \boldsymbol{q}_h^{(1)} \circ \boldsymbol{\phi} \cdot \boldsymbol{n}_1)\|^2_{\mathcal{I}_h^2} \\
&+ 2\|\delta_e^{1/7}\tau^{1/2}u_h^{(1)}\|^2_{\mathcal{I}_h^1} + 4\|f\|^2_{\Omega} + \frac{1}{8}\sum_{i=1}^{2}\|u_h^{(i)}\|^2_{\Omega_h^i} + 2\sum_{i=1}^{2}\|\boldsymbol{g}_i\|^2_{\Omega_h^i} \\
&+ 8\|C_e^{tr}h_e^{-1/2}P_{M^1}f_1\|^2_{\mathcal{I}_h^1} + 2\|\delta_e^{-1/7}\tau^{-1/2}P_{M^2}f_2\|^2_{\mathcal{I}_h^2}. \qquad (3.10)
\end{aligned}$$

By the discrete trace, there exists $C_{tr}^e > 0$ independent of the meshsize, such that $\|h_e^{1/2}u_h^{(1)}\|_e \leq C_{tr}^e\|u_h^{(1)}\|_{K_e}$. Then, the second term can be bounded by $2\max_{e\in\mathcal{I}_h^1}(\delta_e^{2/7}h_e^{-1}\tau)\|u_h^{(1)}\|^2_{\Omega_h^1}$.

Now, by (2.10d) for $F \in \mathcal{F}_h$, there is a constant $\widehat{C}_1 > 0$, such that

$$\|(\boldsymbol{q}_h^{(1)} \circ \boldsymbol{\phi}) \cdot \boldsymbol{n}_1 - \boldsymbol{E}_{\boldsymbol{q}_h^{(1)}} \cdot \boldsymbol{n}_1\|_F \leq \widehat{C}_1 \delta_e \; h_e^{-3/2} C_e^{ext} \|\boldsymbol{q}_h^{(1)}\|_{K_e},$$

where $e = \boldsymbol{\phi}(F) \in \mathcal{I}_h^1$ and K_e is the element where e belongs. Then, from these inequalities and (2.9), we conclude there exists a constant $C_1 > 0$, independent of the meshsize, such that (3.8) holds under Assumption (A.5). □

We observe that we need to provide an estimate for the L^2-norm of $u_h^{(1)}$ and $u_h^{(2)}$. To that end, we will employ a duality argument.

3.2 *A duality argument*

Given $\Theta \in L^2(\Omega)$, we will assume that the solution $(\boldsymbol{\varphi}, \psi)$ of

$$\boldsymbol{\varphi} + \nabla \psi = 0 \qquad \text{in } \Omega, \tag{3.11a}$$

$$\nabla \cdot \boldsymbol{\varphi} = \Theta \qquad \text{in } \Omega, \tag{3.11b}$$

$$\psi = 0 \qquad \text{on } \partial\Omega \tag{3.11c}$$

has regularity

$$\|\boldsymbol{\varphi}\|_{H^1(\Omega)} + \|\psi\|_{H^2(\Omega)} \leq C_{reg} \|\Theta\|_{\Omega}, \tag{3.12}$$

where $C_{reg} > 0$ depends on the domain Ω. This result holds, for instance, for convex polyhedral domains and for domains with C^2-boundaries.

LEMMA 3.6 If Assumption (A) and (3.12) hold true then there exists $C_2 > 0$, independent of the meshsize, such that

$$\sum_{i=1}^{2} \|u_h^{(i)}\|_{\Omega_h^i}^2 \leq C_2 C_{\delta,h} \|(\boldsymbol{q}_h, u_h, \widehat{u}_h, \widetilde{u}_h)\|^2 + \sum_{i=1}^{2} \|P_{M^i} f_i\|_{\mathcal{T}_h^i}^2 + \sum_{i=1}^{2} h_i^{2\min\{1,k\}} \|f\|_{\Omega_h^i}^2 + \sum_{i=1}^{2} h_i^{2\min\{1,k\}} \|\boldsymbol{g}_i\|_{\Omega_h^i}^2, \tag{3.13}$$

where we recall $C_{\delta,h}$ has been defined in Assumption (A.7).

Proof. By the result of (Cockburn *et al.*, 2012, Lemma 3.3) applied to our context, it can be shown that given $\Theta \in L^2(\Omega)$, the solution of (3.11) satisfies

$$\begin{aligned} \sum_{i=1}^{2} (u_h^{(i)}, \Theta)_{\Omega_h^i} = &\sum_{i=1}^{2} (\boldsymbol{q}_h^{(i)}, \boldsymbol{\Pi}_{\boldsymbol{V}^i} \boldsymbol{\varphi} - \boldsymbol{\varphi})_{\Omega_h^i} + \sum_{i=1}^{2} \mathbb{T}_u^i \\ &+ \sum_{i=1}^{2} (f, \Pi_{W^i} \psi)_{\Omega_h^i} + \sum_{i=1}^{2} (\boldsymbol{g}_i, \boldsymbol{\Pi}_{\boldsymbol{V}^i} \boldsymbol{\varphi} - \boldsymbol{\varphi})_{\Omega_h^i} - \sum_{i=1}^{2} (\boldsymbol{g}_i, \nabla \psi - \nabla \Pi_{W^i} \psi)_{\Omega_h^i}, \end{aligned} \tag{3.14}$$

since $\boldsymbol{g}_i$ is orthogonal to polynomials of degree $k-1$. Here, $\mathbb{T}_u^i := \langle \widehat{u}_h^{(i)}, \boldsymbol{\varphi}\cdot\boldsymbol{n}_i\rangle_{\mathcal{I}_h^i} - \langle \widehat{\boldsymbol{q}}_h^{(i)}\cdot\boldsymbol{n}_i, \psi\rangle_{\mathcal{I}_h^i}$ and $(\boldsymbol{\Pi}_{\boldsymbol{V}^i}, \Pi_{W^i})$ is the HDG projection defined in (2.2). Similarly to the ideas behind the proof of Lemma 3.5, we will explicitly write $\mathbb{T}_u^1 + \mathbb{T}_u^2$ in terms of quantities related to the mismatch between $\mathcal{I}_h^1$ and $\mathcal{I}_h^2$. First, we add and subtract $\widetilde{u}_h^{(2)}\circ\boldsymbol{\phi}$, to obtain that

$$\mathbb{T}_u^2 = \langle \widehat{u}_h^{(2)} - \widetilde{u}_h^{(2)}\circ\boldsymbol{\phi}, \boldsymbol{\varphi}\cdot\boldsymbol{n}_2\rangle_{\mathcal{I}_h^2} + \langle \widetilde{u}_h^{(2)}\circ\boldsymbol{\phi}, \boldsymbol{\varphi}\cdot\boldsymbol{n}_2\rangle_{\mathcal{I}_h^2} - \langle \widehat{\boldsymbol{q}}_h^{(2)}\cdot\boldsymbol{n}_2, \psi\rangle_{\mathcal{I}_h^2}.$$

By (3.2a) and employing the definition of L^2-projection P_{M^1},

$$\begin{aligned}\mathbb{T}_u^2 = {} & \langle \widehat{u}_h^{(2)} - \widetilde{u}_h^{(2)}\circ\boldsymbol{\phi}, \boldsymbol{\varphi}\cdot\boldsymbol{n}_2\rangle_{\mathcal{I}_h^2} + \langle \widetilde{u}_h^{(2)}, (Id - P_{M^1})((\boldsymbol{\varphi}\cdot\boldsymbol{n}_2)\circ\boldsymbol{\phi}^{-1})\rangle_{\mathcal{I}_h^1} \\ & + \langle \widehat{u}_h^{(1)}, P_{M^1}((\boldsymbol{\varphi}\cdot\boldsymbol{n}_2)\circ\boldsymbol{\phi}^{-1})\rangle_{\mathcal{I}_h^1} - \langle f_1, P_{M^1}((\boldsymbol{\varphi}\cdot\boldsymbol{n}_2)\circ\boldsymbol{\phi}^{-1})\rangle_{\mathcal{I}_h^1} - \langle \widehat{\boldsymbol{q}}_h^{(2)}\cdot\boldsymbol{n}_2, \psi\rangle_{\mathcal{I}_h^2}.\end{aligned}$$

On the other hand, we add and subtract $\widetilde{q}_h^{(1)}\circ\boldsymbol{\phi}^{-1}$ to deduce that

$$\mathbb{T}_u^1 = \langle \widehat{u}_h^{(1)}, \boldsymbol{\varphi}\cdot\boldsymbol{n}_1\rangle_{\mathcal{I}_h^1} - \langle \widehat{\boldsymbol{q}}_h^{(1)}\cdot\boldsymbol{n}_1 - \widetilde{q}_h^{(1)}\circ\boldsymbol{\phi}^{-1}, \psi\rangle_{\mathcal{I}_h^1} - \langle \widetilde{q}_h^{(1)}\circ\boldsymbol{\phi}^{-1}, \psi\rangle_{\mathcal{I}_h^1}.$$

By (3.2b), (3.6) and the L^2-projection P_{M^2}, we obtain that

$$\begin{aligned}\mathbb{T}_u^1 = {} & \langle \widehat{u}_h^{(1)}, \boldsymbol{\varphi}\cdot\boldsymbol{n}_1\rangle_{\mathcal{I}_h^1} - \langle (\boldsymbol{E}_{\boldsymbol{q}_h^{(1)}}\cdot\boldsymbol{n}_2)\circ\boldsymbol{\phi}^{-1} + \boldsymbol{q}_h^{(1)}\cdot\boldsymbol{n}_1, \psi\rangle_{\mathcal{I}_h^1} \\ & - \langle \widetilde{q}_h^{(1)}, (Id - P_{M^2})(\psi\circ\boldsymbol{\phi})\rangle_{\mathcal{I}_h^2} + \langle \widehat{\boldsymbol{q}}_h^{(2)}\cdot\boldsymbol{n}_2, \psi\circ\boldsymbol{\phi}\rangle_{\mathcal{I}_h^2} - \langle P_{M^2}f_2, \psi\circ\boldsymbol{\phi}\rangle_{\mathcal{I}_h^2}.\end{aligned}$$

Thus,

$$\begin{aligned}\mathbb{T}_u^1 + \mathbb{T}_u^2 = {} & \langle \widehat{u}_h^{(2)} - \widetilde{u}_h^{(2)}\circ\boldsymbol{\phi}, \boldsymbol{\varphi}\cdot\boldsymbol{n}_2\rangle_{\mathcal{I}_h^2} + \langle \widetilde{u}_h^{(2)}, (Id - P_{M^1})((\boldsymbol{\varphi}\cdot\boldsymbol{n}_2)\circ\boldsymbol{\phi}^{-1})\rangle_{\mathcal{I}_h^1} \\ & + \langle \widehat{u}_h^{(1)}, (\boldsymbol{\varphi}\cdot\boldsymbol{n}_2)\circ\boldsymbol{\phi}^{-1} + \boldsymbol{\varphi}\cdot\boldsymbol{n}_1\rangle_{\mathcal{I}_h^1} + \langle \widehat{\boldsymbol{q}}_h^{(2)}\cdot\boldsymbol{n}_2, \psi\circ\boldsymbol{\phi} - \psi\rangle_{\mathcal{I}_h^2} \\ & - \langle (\boldsymbol{E}_{\boldsymbol{q}_h^{(1)}}\cdot\boldsymbol{n}_2)\circ\boldsymbol{\phi}^{-1} + \boldsymbol{q}_h^{(1)}\cdot\boldsymbol{n}_1, \psi\rangle_{\mathcal{I}_h^1} - \langle \widetilde{q}_h^{(1)}, (Id - P_{M^2})(\psi\circ\boldsymbol{\phi})\rangle_{\mathcal{I}_h^2} \\ & - \langle P_{M^1}f_1\circ\boldsymbol{\phi}, \boldsymbol{\varphi}\cdot\boldsymbol{n}_2\rangle_{\mathcal{I}_h^2} - \langle P_{M^2}f_2\circ\boldsymbol{\phi}^{-1}, \psi\rangle_{\mathcal{I}_h^1}.\end{aligned}$$

Finally, we decompose $\widehat{\boldsymbol{q}}_h^{(2)}\cdot\boldsymbol{n}_2$ by using the definition of the flux (2.11e) and identity (3.7). Moreover, by Assumption (A.3), $\boldsymbol{\phi}$ is a piecewise affine mapping; hence, we can get rid of P_{M^2} in the first term and also observe that the second term vanishes. Therefore, rearranging terms, we deduce that

$$\mathbb{T}_u^1 + \mathbb{T}_u^2 =: \sum_{i=1}^{8}\mathbb{S}_i,$$

where

$$\mathbb{S}_1 := -\langle |\sigma|^{-1/2}(\widetilde{u}_h^{(2)} \circ \boldsymbol{\phi} - \widehat{u}_h^{(2)}), |\sigma|^{1/2}(\boldsymbol{\varphi} \circ \boldsymbol{\phi}) \cdot \boldsymbol{n}_2 + |\sigma|^{-1/2}(-\psi \circ \boldsymbol{\phi} + \psi)\rangle_{\mathcal{I}_h^2},$$

$$\mathbb{S}_2 := \langle \widehat{u}_h^{(1)}, (\boldsymbol{\varphi} \cdot \boldsymbol{n}_2) \circ \boldsymbol{\phi}^{-1} + \boldsymbol{\varphi} \cdot \boldsymbol{n}_1 \rangle_{\mathcal{I}_h^1},$$

$$\mathbb{S}_3 := \langle (\boldsymbol{q}_h^{(1)} \circ \boldsymbol{\phi}) \cdot \boldsymbol{n}_2 - \boldsymbol{E}_{\boldsymbol{q}_h^{(1)}} \cdot \boldsymbol{n}_2, \psi \circ \boldsymbol{\phi} \rangle_{\mathcal{I}_h^2}, \qquad \mathbb{S}_4 := -\langle \Lambda^{(2)}_{\boldsymbol{q}_h^{(2)}}, \psi \circ \boldsymbol{\phi} - \psi \rangle_{\mathcal{I}_h^2},$$

$$\mathbb{S}_5 := \langle \tau^{1/2}(u_h^{(2)} - \widehat{u}_h^{(2)}), \tau^{1/2}(\psi \circ \boldsymbol{\phi} - \psi) \rangle_{\mathcal{I}_h^2}, \qquad \mathbb{S}_6 := -\langle \widetilde{q}_h^{(1)}, (Id - P_{M^2})(\psi \circ \boldsymbol{\phi}) \rangle_{\mathcal{I}_h^2},$$

$$\mathbb{S}_7 := -\langle P_{M^1} f_1 \circ \boldsymbol{\phi}, \boldsymbol{\varphi} \cdot \boldsymbol{n}_2 \rangle_{\mathcal{I}_h^2}, \qquad \mathbb{S}_8 := -\langle P_{M^2} f_2, \psi \circ \boldsymbol{\phi} \rangle_{\mathcal{I}_h^2}.$$

We now bound each of these terms by the Cauchy–Schwarz inequality, the estimates in Lemma 2.1 and the regularity Assumption 3.12:

$$\mathbb{S}_1 \lesssim \delta \, \| |\sigma|^{-1/2}(\widetilde{u}_h^{(2)} \circ \boldsymbol{\phi} - \widehat{u}_h^{(2)}) \|_{\mathcal{I}_h^2} \, \| \Theta \|_{\Omega},$$

$$\mathbb{S}_2 \lesssim \| \delta_e^{1/7} \tau^{1/2} \widehat{u}_h^{(1)} \|_{\mathcal{I}_h^1} \max_{e \in \mathcal{I}_h^1} (\delta_e^{-1/7} \tau^{-1/2} \, \delta_e^{1/2}) \| \Theta \|_{\Omega}, \quad \mathbb{S}_3 \lesssim \max_{e \in \mathcal{I}_h^2} (\delta_e \; h_e^{-3/2} C_e^{ext}) \, \| \boldsymbol{q}_h^{(1)} \|_{\Omega_h^1} \| \Theta \|_{\Omega},$$

$$\mathbb{S}_4 \lesssim \delta^{1/2} \| |\sigma|^{1/2} \Lambda^{(2)}_{\boldsymbol{q}_h^{(2)}} \|_{\mathcal{I}_h^2} \| \Theta \|_{\Omega}, \qquad \mathbb{S}_5 \lesssim \delta \, \tau^{1/2} \| \tau^{1/2}(u_h^{(2)} - \widehat{u}_h^{(2)}) \|_{\mathcal{I}_h^2} \| \Theta \|_{\Omega},$$

$$\mathbb{S}_7 \lesssim \| P_{M^1} f_1 \|_{\mathcal{I}_h^1} \| \Theta \|_{\Omega}, \qquad \mathbb{S}_8 \lesssim \| P_{M^2} f_2 \|_{\mathcal{I}_h^2} \| \Theta \|_{\Omega}.$$

For $\mathbb{S}_6$, by the definition of $\widetilde{q}_h^{(1)}$ in (2.14b), the approximation property of the L^2-projection P_{M^2}, the discrete trace inequality and (2.7), we have

$$\begin{aligned}
\mathbb{S}_6 &\leq \| h_e \widetilde{q}_h^{(1)} \|_{\mathcal{I}_h^2} \| h_e^{-1}(Id - P_{M^2})(\psi \circ \boldsymbol{\phi}) \|_{\mathcal{I}_h^2} \lesssim \| h_e \widetilde{q}_h^{(1)} \|_{\mathcal{I}_h^2} \| \psi \|_{H^2(\Omega)} \\
&\lesssim \left(\| h_e \boldsymbol{E}_{\boldsymbol{q}_h^{(1)}} \cdot \boldsymbol{n}_2 \|_{\mathcal{I}_h^2} + \| h_e \tau (u_h^{(1)} - \widehat{u}_h^{(1)}) \|_{\mathcal{I}_h^1} \right) \| \Theta \|_{\Omega} \\
&\lesssim \left(\delta^{1/2} \| \boldsymbol{q}_h^{(1)} \|_{\Omega_h^1} + h \tau^{1/2} \| \tau^{1/2}(u_h^{(1)} - \widehat{u}_h^{(1)}) \|_{\mathcal{I}_h^1} \right) \| \Theta \|_{\Omega}.
\end{aligned}$$

In summary, combining (3.14) with the bound for $\mathbb{S}_i$ $(i = 1, ..., 8)$ and noticing that

$$\| \boldsymbol{\Pi}_{\boldsymbol{V}^i} \boldsymbol{\varphi} - \boldsymbol{\varphi} \|_{\Omega_h^i} + \| \nabla \psi - \nabla \Pi_{W^i} \psi \|_{\Omega_h^i} \leq C_{reg} h_i^{\min\{1,k\}} \| \Theta \|_{\Omega},$$

by (2.3), and considering (2.9a), we obtain

$$\sum_{i=1}^{2}(u_h^{(i)},\Theta)_{\Omega_h^i} \lesssim \|\Theta\|_{\Omega}\Bigg(\delta+\max_{e\in\mathcal{I}_h^2}(\delta_e^{5/14}\tau^{-1/2})+\max_{e\in\mathcal{I}_h^2}\delta_e h_e^{-3/2}C_e^{ext}+\delta^{1/2}\max_{e\in\mathcal{I}_h^2}\delta_e^{3/2}h_e^{-3/2}C_e^{ext}C_e^{inv}$$
$$+\delta\tau^{1/2}+\delta^{1/2}+h\tau^{1/2}+h_1^{\min\{1,k\}}+h_2^{\min\{1,k\}}\Bigg)\|(\boldsymbol{q}_h,u_h,\widehat{u}_h,\widetilde{u}_h)\|$$
$$+\left(\sum_{i=1}^{2}\|P_{M^i}f_i\|_{\mathcal{I}_h^i}+\sum_{i=1}^{2}h_i^{\min\{1,k\}}\|f\|_{\Omega_h^i}+\sum_{i=1}^{2}h_i^{\min\{1,k\}}\|\boldsymbol{g}_i\|_{\Omega_h^i}\right)\|\Theta\|_{\Omega}.$$

Then, we take $\Theta=\begin{cases}u_h^{(1)} & \text{in} \quad \Omega_h^1\\ u_h^{(2)} & \text{in} \quad \Omega_h^2\end{cases}$ and we conclude that there exists $C_2>0$, independent of the meshsize, such that

$$\sum_{i=1}^{2}\|u_h^{(i)}\|_{\Omega_h^i}^2 \le C_2\Bigg(\max_{e\in\mathcal{I}_h^2}(\delta_e^{5/7}\tau^{-1})+\max_{e\in\mathcal{I}_h^2}\delta_e^2h_e^{-3}(C_e^{ext})^2$$
$$+\delta\tau+\delta+h^2\tau+h_1^{2\min\{1,k\}}+h_2^{2\min\{1,k\}}\Bigg)\|(\boldsymbol{q}_h,u_h,\widehat{u}_h,\widetilde{u}_h)\|^2$$
$$+\sum_{i=1}^{2}\|P_{M^i}f_i\|_{\mathcal{I}_h^i}^2+\sum_{i=1}^{2}h_i^{2\min\{1,k\}}\|f\|_{\Omega_h^i}^2+\sum_{i=1}^{2}h_i^{2\min\{1,k\}}\|\boldsymbol{g}_i\|_{\Omega_h^i}^2,$$

where we have also used the facts that $\delta_e^3h_e^{-3}$ is bounded by Assumption (A.5) and $\delta^2\le\delta$. Thus, the result follows. □

3.3 *Proof of Theorem* 3.1

Proof. We first employ the estimate obtained in Lemma 3.6 to bound the third term of the right-hand side of (3.8), to obtain that

$$\left(1-C_{\delta,h}\max_{e\in\mathcal{I}_h^1}(\delta_e^{2/7}h_e^{-1}\tau)\right)\|(\boldsymbol{q}_h,u_h,\widehat{u}_h,\widetilde{u}_h)\|^2\lesssim\|f\|_{\Omega}^2+\sum_{i=1}^{2}\|\boldsymbol{g}_i\|_{\Omega_h^i}^2+\|h_e^{-1/2}P_{M^1}f_1\|_{\mathcal{I}_h^1}^2+\|\delta_e^{1/7}P_{M^2}f_2\|_{\mathcal{I}_h^2}^2,$$

with $C_{\delta,h}=C_1\left(\max_{e\in\mathcal{I}_h^2}\delta_e^{5/7}+\max_{e\in\mathcal{I}_h^2}\delta_e^2h_e^{-3}(C_e^{ext})^2+\delta+h_1^2+h_2^2\right)$, since $\delta<1$, τ is of order one, $k\ge1$ and $h<1$. Thus, (3.5a) follows by Assumption (A.7). In addition, by Lemma 3.6, we obtain (3.5b). □

4. Error estimates

Let us proceed now to derive the error estimates of the proposed method. To that end, we employ the stability estimate deduced in previous sections.

Let us consider the solution $(\boldsymbol{q}, u)$ of (1.1). For $i \in \{1,2\}$, we introduce the projection of the errors $\boldsymbol{\varepsilon}^{\boldsymbol{q}^{(i)}} := \boldsymbol{\Pi}_{\boldsymbol{V}^i}\boldsymbol{q} - \boldsymbol{q}_h^{(i)}$, $\varepsilon^{u^{(i)}} := \Pi_{W^i}u - u_h^{(i)}$, $\varepsilon^{\widehat{u}^{(i)}} := P_{M^i}u - \widehat{u}_h^{(i)}$, $\boldsymbol{\varepsilon}^{\widehat{\boldsymbol{q}}^{(i)}} \cdot \boldsymbol{n}_i := P_{M^i}(\boldsymbol{q}\cdot\boldsymbol{n}_i) - \widehat{\boldsymbol{q}}_h^{(i)} \cdot \boldsymbol{n}_i$, where we P_{M^i} is the L^2 projection into M_h^i, and the error of the projections $\boldsymbol{I}^{\boldsymbol{q}^{(i)}} := \boldsymbol{q} - \boldsymbol{\Pi}_{\boldsymbol{V}^i}\boldsymbol{q}$ and $I^{u^{(i)}} := u - \Pi_{W^i}u$. Using these quantities, we can decompose the HDG error $\boldsymbol{q} - \boldsymbol{q}_h^{(i)} = \boldsymbol{\varepsilon}^{\boldsymbol{q}^{(i)}} + \boldsymbol{I}^{\boldsymbol{q}^{(i)}}$ and $u - u_h^{(i)} = \varepsilon^{u^{(i)}} + I^{u^{(i)}}$.

LEMMA 4.1 The projection of the errors satisfies

$$(\boldsymbol{\varepsilon}^{\boldsymbol{q}^{(i)}}, \boldsymbol{v})_{\Omega_h^i} - (\varepsilon^{u^{(i)}}, \nabla\cdot\boldsymbol{v})_{\Omega_h^i} + \langle \widehat{u}_h^{(i)}, \boldsymbol{v}\cdot\boldsymbol{n}_i\rangle_{\partial\Omega_h^i} = -(\boldsymbol{I}^{\boldsymbol{q}^{(i)}}, \boldsymbol{v})_{\Omega_h^i}, \tag{4.1a}$$

$$-(\boldsymbol{\varepsilon}^{\boldsymbol{q}^{(i)}}, \nabla w)_{\Omega_h^i} + \langle \boldsymbol{\varepsilon}^{\widehat{\boldsymbol{q}}^{(i)}}\cdot\boldsymbol{n}_i, w\rangle_{\partial\Omega_h^i} = 0 \tag{4.1b}$$

$$\langle \boldsymbol{\varepsilon}^{\widehat{\boldsymbol{q}}^{(i)}}\cdot\boldsymbol{n}_i, \mu\rangle_{\partial\Omega_h^i\setminus\Gamma_h^i} = 0, \tag{4.1c}$$

$$\langle \varepsilon^{\widehat{u}^{(i)}}, \mu\rangle_{\Gamma_h^i\setminus\mathcal{I}_h^i} = 0, \tag{4.1d}$$

for all $(\boldsymbol{v}, w, \mu) \in \boldsymbol{V}_h^i \times W_h^i \times M_h^i$ and

$$\boldsymbol{\varepsilon}^{\widehat{\boldsymbol{q}}^{(i)}}\cdot\boldsymbol{n}_i = \boldsymbol{\varepsilon}^{\boldsymbol{q}^{(i)}}\cdot\boldsymbol{n}_i + \tau(\varepsilon^{u^{(i)}} - \varepsilon^{\widehat{u}^{(i)}}) \qquad \text{on} \quad \partial\Omega_h^i. \tag{4.1e}$$

Moreover, for $\boldsymbol{x}_1 \in \mathcal{I}_h^1$, let

$$\varepsilon^{\widetilde{u}^{(2)}}(\boldsymbol{x}_1) := \varepsilon^{\widehat{u}^{(2)}}(\boldsymbol{x}_2) - |\sigma(\boldsymbol{x}_2)|\int_0^1 \boldsymbol{E}_{\boldsymbol{\varepsilon}^{\boldsymbol{q}^{(2)}}}(\boldsymbol{x}(s))\cdot\boldsymbol{n}_2\,\mathrm{d}s$$

and $\varepsilon^{\widetilde{q}^{(1)}}(\boldsymbol{x}_2) := -(\boldsymbol{E}_{\boldsymbol{\varepsilon}^{\boldsymbol{q}^{(1)}}}\cdot\boldsymbol{n}_2)(\boldsymbol{x}_2) + \tau(\varepsilon^{u^1} - \varepsilon^{\widehat{u}^{(1)}})(\boldsymbol{\phi}(\boldsymbol{x}_2))$ for $\boldsymbol{x}_2 \in \mathcal{I}_h^2$. They satisfy

$$\begin{aligned}\langle \varepsilon^{\widehat{u}^{(1)}} - \varepsilon^{\widetilde{u}^{(2)}}, \mu\rangle_{\mathcal{I}_h^1} &= \langle P_{M^1}(u\circ\boldsymbol{\phi}^{-1}) - (P_{M^2}u)\circ\boldsymbol{\phi}^{-1}, \mu\rangle_{\mathcal{I}_h^1} - \langle|\sigma|\Lambda^{(2)}_{\boldsymbol{I}^{\boldsymbol{q}^{(2)}}}\circ\boldsymbol{\phi}^{-1}, \mu\rangle_{\mathcal{I}_h^1}\\ &\quad - \langle|\sigma|\boldsymbol{I}^{\boldsymbol{q}^{(2)}}\circ\boldsymbol{\phi}^{-1}, \mu\rangle_{\mathcal{I}_h^1} \qquad \forall\,\mu\in M_h^1,\end{aligned} \tag{4.1f}$$

$$\langle \boldsymbol{\varepsilon}^{\widehat{\boldsymbol{q}}^{(2)}}\cdot\boldsymbol{n}_2 + \varepsilon^{\widetilde{q}^{(1)}}, \mu\rangle_{\mathcal{I}_h^2} = \langle(\boldsymbol{I}^{\boldsymbol{q}^{(1)}} - \boldsymbol{I}^{\boldsymbol{q}^{(1)}}\circ\boldsymbol{\phi})\cdot\boldsymbol{n}_1, \mu\rangle_{\mathcal{I}_h^2} \qquad \forall\,\mu\in M_h^2. \tag{4.1g}$$

Proof. The identities (4.1a)–(4.1e) follow directly from the definition of the projection of the errors and (2.11). Now, let $\boldsymbol{x}_1 \in \mathcal{I}_h^1$. By (2.14a) and (2.1), we rewrite

$$\begin{aligned}\varepsilon^{\widetilde{u}^{(2)}}(\boldsymbol{x}_1) &= (P_{M^2}u)(\boldsymbol{x}_2) - \widehat{u}_h^{(2)}(\boldsymbol{x}_2) - |\sigma(\boldsymbol{x}_2)|\int_0^1 \boldsymbol{\Pi}_{\boldsymbol{V}^2}\boldsymbol{q}(\boldsymbol{x}(s))\cdot\boldsymbol{n}_2\,\mathrm{d}s + |\sigma(\boldsymbol{x}_2)|\int_0^1 \boldsymbol{q}_h^{(2)}(\boldsymbol{x}(s))\cdot\boldsymbol{n}_2\,\mathrm{d}s\\ &= (P_{M^2}u)(\boldsymbol{x}_2) - |\sigma(\boldsymbol{x}_2)|\int_0^1 \boldsymbol{\Pi}_{\boldsymbol{V}^2}\boldsymbol{q}(\boldsymbol{x}(s))\cdot\boldsymbol{n}_2\,\mathrm{d}s - \widetilde{u}_h^{(2)}(\boldsymbol{x}_1).\end{aligned}$$

On the other hand, by (2.13), we obtain

$$u(\boldsymbol{x}_1) - \varepsilon^{\widetilde{u}^{(2)}}(\boldsymbol{x}_1) = u(\boldsymbol{x}_2) - (P_{M^2}u)(\boldsymbol{x}_2) - |\sigma(\boldsymbol{x}_2)| \int_0^1 \boldsymbol{I}^{\boldsymbol{q}^{(2)}}(\boldsymbol{x}(s)) \cdot \boldsymbol{n}_2 \, \mathrm{d}s + \widetilde{u}_h^{(2)}(\boldsymbol{x}_1)$$
$$= u(\boldsymbol{x}_2) - (P_{M^2}u)(\boldsymbol{x}_2) - |\sigma(\boldsymbol{x}_2)| \Lambda^{(2)}_{\boldsymbol{I}^{\boldsymbol{q}^{(2)}}}(\boldsymbol{x}_2) - |\sigma(\boldsymbol{x}_2)| \boldsymbol{I}^{\boldsymbol{q}^{(2)}}(\boldsymbol{x}_2) + \widetilde{u}_h^{(2)}(\boldsymbol{x}_1),$$

where in the last identity we added and subtracted $\boldsymbol{I}^{\boldsymbol{q}^{(2)}}(\boldsymbol{x}_2)$ and considered the definition in (2.8). Hence, for $\mu \in M_h^1$, the above expression together with (2.12a) and the definition of the L^2-projection P_{M^1} imply

$$\langle \varepsilon^{\widehat{u}^{(1)}} - \varepsilon^{\widetilde{u}^{(2)}}, \mu \rangle_{\mathcal{I}_h^1} = \langle u \circ \boldsymbol{\phi}^{-1} - (P_{M^2}u) \circ \boldsymbol{\phi}^{-1} - |\sigma| \Lambda^{(2)}_{\boldsymbol{I}^{\boldsymbol{q}^{(2)}}} \circ \boldsymbol{\phi}^{-1} - |\sigma| \boldsymbol{I}^{\boldsymbol{q}^{(2)}} \circ \boldsymbol{\phi}^{-1}, \mu \rangle_{\mathcal{I}_h^1}$$

and (4.1f) follows. Now, let $\boldsymbol{x}_2 \in \mathcal{I}_h^2$. By the definition of the projection of the errors, (2.14b) and (2.2c), it can be shown that

$$\varepsilon^{\widetilde{q}^{(1)}}(\boldsymbol{x}_2) = -\widetilde{q}_h^{(1)}(\boldsymbol{x}_2) - (\boldsymbol{q} \cdot \boldsymbol{n}_2)(\boldsymbol{x}_2) + (\boldsymbol{I}^{\boldsymbol{q}^{(1)}} \cdot \boldsymbol{n}_1)(\boldsymbol{x}_2) + P_{M^1}(\boldsymbol{q} \cdot \boldsymbol{n}_1)(\boldsymbol{\phi}(\boldsymbol{x}_2))$$
$$- (\boldsymbol{q} \cdot \boldsymbol{n}_1)(\boldsymbol{\phi}(\boldsymbol{x}_2)) + (\boldsymbol{I}^{\boldsymbol{q}^{(1)}} \cdot \boldsymbol{n}_1)(\boldsymbol{\phi}(\boldsymbol{x}_2)).$$

Then, let $\mu \in M_h^2$. By (2.12b), (2.2c), (2.11e) and the definition of the L^2-projection P_{M^2}, we have

$$\langle \boldsymbol{\varepsilon}^{\widehat{\boldsymbol{q}}^{(2)}} \cdot \boldsymbol{n}_2 + \varepsilon^{\widetilde{q}^{(1)}}, \mu \rangle_{\mathcal{I}_h^2} = \langle (\boldsymbol{I}^{\boldsymbol{q}^{(1)}} - \boldsymbol{I}^{\boldsymbol{q}^{(1)}} \circ \boldsymbol{\phi}) \cdot \boldsymbol{n}_1, \mu \rangle_{\mathcal{I}_h^2} + \langle P_{M^1}(\boldsymbol{q} \cdot \boldsymbol{n}_1) - \boldsymbol{q} \cdot \boldsymbol{n}_1, \mu \circ \boldsymbol{\phi}^{-1} \rangle_{\mathcal{I}_h^1}.$$

Thus, (4.1g) follows from the fact that $\mu \circ \boldsymbol{\phi}^{-1} \in M_h^1$. □

We observe that the above equations are similar to that of our HDG scheme, where $\boldsymbol{I}^{\boldsymbol{q}^{(i)}}$ and 0 play the role of $\boldsymbol{g}_i$ and f, respectively. Moreover, $f_1 = (u - P_{M^2}u) \circ \boldsymbol{\phi}^{-1} - |\sigma| \Lambda^{(2)}_{\boldsymbol{I}^{\boldsymbol{q}^{(2)}}} \circ \boldsymbol{\phi}^{-1} - |\sigma| \boldsymbol{I}^{\boldsymbol{q}^{(2)}} \circ \boldsymbol{\phi}^{-1}$ and $f_2 = (\boldsymbol{I}^{\boldsymbol{q}^{(1)}} - \boldsymbol{I}^{\boldsymbol{q}^{(1)}} \circ \boldsymbol{\phi}) \cdot \boldsymbol{n}_1$. Hence, we consider the result in Theorem 3.1 applied to this context. To that end, we notice that

$$\|h_e^{-1/2} P_{M^1} f_1\|^2_{\mathcal{I}_h^1} \leq \|h_e^{-1/2}(P_{M^1}(u \circ \boldsymbol{\phi}) - (P_{M^2}u) \circ \boldsymbol{\phi})\|^2_{\mathcal{I}_h^1} + \|h_e^{-1/2} |\sigma| \Lambda^{(2)}_{\boldsymbol{I}^{\boldsymbol{q}^{(2)}}} \circ \boldsymbol{\phi}^{-1}\|^2_{\mathcal{I}_h^1}$$
$$+ \|h_e^{-1/2} |\sigma| \boldsymbol{I}^{\boldsymbol{q}^{(2)}} \circ \boldsymbol{\phi}^{-1}\|^2_{\mathcal{I}_h^1}. \tag{4.2}$$

We observe that the first term would vanish if each face in $\mathcal{I}_h^2$ is mapped to a single face in $\mathcal{I}_h^1$. Otherwise, it can be bounded using the approximation properties of the L^2-projection over M_h^1. That is, there exists a constant $C_{nc} \geq 0$, independent of h, such that

$$\|h_e^{-1/2}(P_{M^1}(u \circ \boldsymbol{\phi}) - (P_{M^2}u) \circ \boldsymbol{\phi})\|^2_{\mathcal{I}_h^1} \leq C_{nc} h^{2l_u+1} |u|^2_{H^{l_u+1}(\Omega)}.$$

The constant C_{nc} takes into account the 'nonconformity' between the computational interfaces, and it is zero when $\mathcal{I}_h^2$ is mapped to a single face in $\mathcal{I}_h^1$. Then,

$$\|h_e^{-1/2} P_{M^1} f_1\|_{\mathcal{I}_h^1}^2 \lesssim C_{nc} h^{2l_u+1} |u|_{H^{l_u+1}(\Omega)}^2 + \max_{e\in\mathcal{I}_h^2}(\delta_e^4 h_e^{-4}) \|\boldsymbol{I}^{\boldsymbol{q}^{(2)}}\|_{\Omega_h^2}^2 + \max_{e\in\mathcal{I}_h^2}(\delta_e h_e^{-1}) \|\boldsymbol{I}^{\boldsymbol{q}^{(2)}}\|_{\Omega_h^2}^2, \tag{4.3}$$

where we used the estimate in (2.9) and a scaling argument to bound the $L^2(\mathcal{I}_h^1)$-norm of $\boldsymbol{I}^{\boldsymbol{q}^{(2)}}$ in terms of its $L^2(\Omega_h^1)$-norm. By Assumption (A) the terms $(\delta_e^4 h_e^{-4})$ and $\delta_e h_e^{-1}$ are bounded, then

$$\|h_e^{-1/2} P_{M^1} f_1\|_{\mathcal{I}_h^1}^2 \lesssim C_{nc} h^{2l_u+1} |u|_{H^{l_u+1}(\Omega)}^2 + \|\boldsymbol{I}^{\boldsymbol{q}^{(2)}}\|_{\Omega_h^2}^2.$$

Moreover, by (2.10c),

$$\|\delta_e^{1/7} P_{M^2} f_2\|_{\mathcal{I}_h^2}^2 \le \|\delta_e^{1/7} |\sigma|^{1/2} |\sigma|^{-1/2} P_{M^2} f_2\|_{\mathcal{I}_h^2}^2 \le \delta^{9/7} |\boldsymbol{I}^{\boldsymbol{q}^{(2)}}|_{\boldsymbol{H}^1(\Omega_h^2)}^2. \tag{4.4}$$

Then, by the stability estimate (3.5a) applied to (4.1), we obtain

$$\|(\boldsymbol{\varepsilon}^{\boldsymbol{q}}, \varepsilon^{u^{(i)}}, \varepsilon^{\widehat{u}}, \varepsilon^{\widetilde{u}^{(2)}})\|^2 \lesssim \|\boldsymbol{I}^{\boldsymbol{q}^{(1)}}\|_{\Omega_h^1}^2 + \|\boldsymbol{I}^{\boldsymbol{q}^{(2)}}\|_{\Omega_h^2}^2 + \delta^{9/7} |\boldsymbol{I}^{\boldsymbol{q}^{(2)}}|_{\boldsymbol{H}^1(\Omega_h^2)}^2 + C_{nc} h^{2l_u+1} |u|_{H^{l_u+1}(\Omega)}^2. \tag{4.5}$$

Moreover, by (3.5b), (4.3) and (4.4),

$$\begin{aligned}\sum_{i=1}^{2} \|\varepsilon^{u^{(i)}}\|_{\Omega_h^i}^2 \lesssim C_{\delta,h} \|(\boldsymbol{\varepsilon}^{\boldsymbol{q}}, \varepsilon^{u^{(i)}}, \varepsilon^{\widehat{u}}, \varepsilon^{\widetilde{u}^{(2)}})\|^2 + h_1^2 \|\boldsymbol{I}^{\boldsymbol{q}^{(1)}}\|_{\Omega_h^1}^2 + \delta |\boldsymbol{I}^{\boldsymbol{q}^{(2)}}|_{\boldsymbol{H}^1(\Omega_h^2)}^2 \\ + \max_{e\in\mathcal{I}_h^2}(\delta_e^4 h_e^{-3} + \delta + h_2^2) \|\boldsymbol{I}^{\boldsymbol{q}^{(2)}}\|_{\Omega_h^2}^2 + C_{nc} h^{2(l_u+1)} |u|_{H^{l_u+1}(\Omega)}^2.\end{aligned} \tag{4.6}$$

Finally, by (4.5) and (4.6) and the properties of the HDG projectors (cf. (2.3)), we obtain the following result.

THEOREM 4.2 Suppose Assumption A and elliptic regularity hold true. If τ is of order one, $k \ge 1$ and $(\boldsymbol{q}, u) \in \boldsymbol{H}^{l_{\boldsymbol{q}}+1}(\Omega) \times H^{l_u+1}(\Omega)$ for $l_{\boldsymbol{q}}, l_u \in [0, k]$ then there exists $h_0 \in (0, 1)$, such that for all $h < h_0$, it holds

$$\left(\sum_{i=1}^{2} \|\boldsymbol{q} - \boldsymbol{q}_h^{(i)}\|_{\Omega_h^i}^2\right)^{1/2} \lesssim h^{(l_{\boldsymbol{q}}+1)} |\boldsymbol{q}|_{\boldsymbol{H}^{l_{\boldsymbol{q}}+1}(\Omega)} + C_{nc}^{1/2} h^{l_u+1/2} |u|_{H^{l_u+1}(\Omega)} + \delta^{9/14} h^{l_{\boldsymbol{q}}} |\boldsymbol{q}|_{\boldsymbol{H}^{l_{\boldsymbol{q}}+1}(\Omega)},$$

$$\left(\sum_{i=1}^{2} \|\varepsilon^{u^{(i)}}\|_{\Omega_h^i}^2\right)^{1/2} \lesssim h^{l_{\boldsymbol{q}}} \left(h^2 + h\delta^{1/2} + hC_{\delta,h}^{1/2} + \delta^{9/14}\right) |\boldsymbol{q}|_{\boldsymbol{H}^{l_{\boldsymbol{q}}+1}(\Omega)} + C_{nc}^{1/2} h^{l_u+1/2} (h^{1/2} + C_{\delta,h}^{1/2}) |u|_{H^{l_u+1}(\Omega)},$$

$$\left(\sum_{i=1}^{2} \|u - u_h^{(i)}\|_{\Omega_h^i}^2\right)^{1/2} \lesssim \left(\sum_{i=1}^{2} \|\varepsilon^{u^{(i)}}\|_{\Omega_h^i}^2\right)^{1/2} + \left(\sum_{i=1}^{2} h_i^{2(l_u+1)} |u|_{H^{l_u+1}(\Omega)}^2\right)^{1/2}.$$

COROLLARY 4.3 Suppose the same assumptions of Theorem 4.2 hold and $(\boldsymbol{q}, u) \in \boldsymbol{H}^{k+1}(\Omega) \times H^{k+1}(\Omega)$. Let $\delta = C_g h^{1+\gamma}$ with $C_g \geq 0$ and $\gamma \in (3/4, 1]$. It holds that

$$\left(\sum_{i=1}^{2} \|\boldsymbol{q} - \boldsymbol{q}_h^{(i)}\|_{\Omega_h^i}^2\right)^{1/2} \lesssim C_{nc} h^{k+1/2} + h^{k+1},$$

$$\left(\sum_{i=1}^{2} \|u - u_h^{(i)}\|_{\Omega_h^i}^2\right)^{1/2} \lesssim h^{k+1}\left(1 + C_g^{1/2} + C_{nc}^{1/2} + C_{nc}^{1/2} C_g^{1/2} h^{\gamma-1}\right),$$

$$\left(\sum_{i=1}^{2} \|\varepsilon^{u^{(i)}}\|_{\Omega_h^i}^2\right)^{1/2} \lesssim h^{k+1}\left(h + C_g^{1/2} + C_{nc}^{1/2} + C_{nc}^{1/2} C_g^{1/2} h^{\gamma-1}\right).$$

REMARK 4.4 The loss of half a power in the error estimate for $\boldsymbol{q}$ is due to the presence of $\langle u - P_{M^2} u, \mu \circ \boldsymbol{\phi}\rangle_{\mathcal{I}_h^2}$ in (4.1f). If this term vanishes, that is $C_{nc} = 0$, as it happens in the case where each face in $\mathcal{I}_h^2$ is mapped to a single face in $\mathcal{I}_h^1$, the L^2-norm of the error in $\boldsymbol{q}$ is of order h^{k+1}. Similarly, the loss of superconvergence in $\varepsilon^{u^{(i)}}$ is due to not only the $\langle u - P_{M^2} u, \mu \circ \boldsymbol{\phi}\rangle_{\mathcal{I}_h^2}$, but also to the presence of the gap. However, the numerical experiments, showed in next section, suggest that superconvergence is attained when δ is of order h^2 (i.e., $\gamma = 1$).

We finish this section by showing the error estimates of a postprocessing of $u_h^{(i)}$ $(i = 1, 2)$. In particular, as introduced by Stenberg (1991), it is possible to define a locally post-processed function $(u_h^*)^{(i)}$ to be the piecewise polynomial function satisfying, for all $K \in \Omega_h^i$,

$$(u_h^*)^{(i)} \in \mathbb{P}_{k+1}(K)$$

$$(\nabla(u_h^*)^{(i)}, \nabla w_h)_K = (\boldsymbol{q}_h^i, \nabla w_h)_K \quad \forall\, w_h \in \mathbb{P}_{k+1}(K), \tag{4.7a}$$

$$((u_h^*)^{(i)}, 1)_K = (u_h^{(i)}, 1)_K. \tag{4.7b}$$

In addition, under the assumptions of Corollary 4.3, the post-processed solution satisfies (cf. Cheung *et al.*, 2019)

$$\|u - (u_h^*)^{(i)}\|_{\Omega_h^i} \lesssim \|\varepsilon^{u^{(i)}}\|_{\Omega_h^i} + h_i \|\boldsymbol{q}^{(i)} - \boldsymbol{q}_h^{(i)}\|_{\Omega_h^i} + h_i^{k+2} |\boldsymbol{q}|_{\boldsymbol{H}^{k+1}(\Omega_h^i)}.$$

Then, by (4.6), (2.3a) and Corollary (4.3),

$$\sum_{i=1}^{2} \|u - (u_h^*)^{(i)}\|_{\Omega_h^i}^2 \lesssim h^{k+1}\left(h + C_g^{1/2} + C_{nc}^{1/2} + C_{nc}^{1/2} C_g^{1/2} h^{\gamma-1}\right). \tag{4.8}$$

5. Numerical results

We consider five numerical examples to illustrate the convergence rates of the method. For all the examples, we consider the physical domain Ω to be a square $[0, 1] \times [0, 1]$, which is approached by two

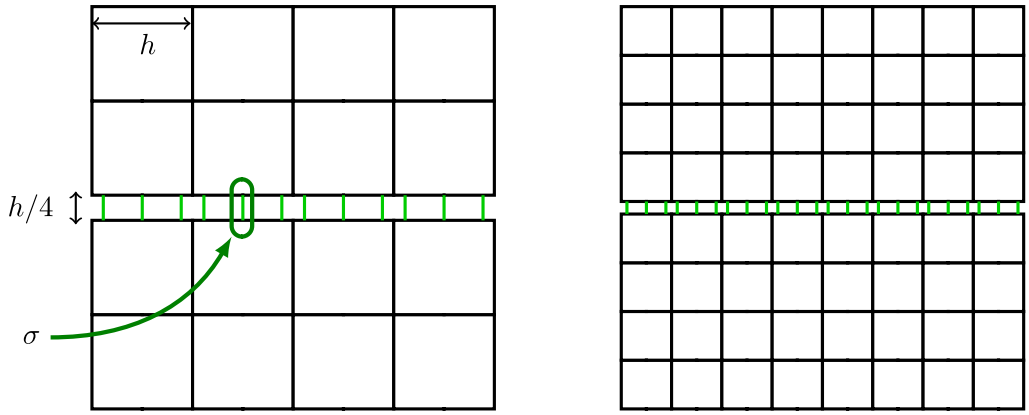

FIG. 5. Two of the meshes used for the third numerical example, with $\delta = h/4$ and flat interfaces. $h = 1/4$ for the left mesh and $h = 1/8$ for the right one. Note the connecting segments σ at the interface Gauss points drawn in green (here, $k = 2$).

computational subdomains $\Omega_h^1 \cup \Omega_h^2$. The five examples differ in the way the two subdomains are geometrically interfaced. We use the same manufactured solution $u(x, y) = \sin(\pi x)\ \sin\left[\pi(-0.2y^2 + 1.2y)\right]$, for all the numerical tests. The forcing term f and the homogeneous Dirichlet boundary conditions applied on $x = \pm 1$ and $y = \pm 1$ are derived from this exact solution. The stabilization parameter τ is always set equal to one. Following Cockburn *et al.* (2012, 2014), we compute the errors

$$e_{\boldsymbol{q}} := \frac{1}{|\Omega_h|^{1/2}} \left(\sum_{i=1}^{2} \|\boldsymbol{q}^{(i)} - \boldsymbol{q}_h^{(i)}\|_{\Omega_h^i}^2 \right)^{1/2}, \quad e_u := \frac{1}{|\Omega_h|^{1/2}} \left(\sum_{i=1}^{2} \|u^{(i)} - u_h^{(i)}\|_{\Omega_h^i}^2 \right)^{1/2}$$

$$e_{u^*} := \frac{1}{|\Omega_h|^{1/2}} \left(\sum_{i=1}^{2} \|u^{(i)} - (u_h^*)^{(i)}\|_{\Omega_h^i}^2 \right)^{1/2},$$

where $|\Omega_h| = |\Omega_h^1| + |\Omega_h^2|$ is the total area of the computational domain. In addition, for each variable, we compute the experimental order of convergence defined as e.o.c. $= \log\left(e_{h_I}/e_{h_{II}}\right)/(h_I/h_{II})$, where e_{h_I} and $e_{h_{II}}$ are the errors associated with the corresponding variable considering two consecutive meshes with h_I and h_{II} element sizes, respectively.

5.1 *Test cases with gap $\delta = \mathcal{O}(h^2)$*

For the first test, Ω_h^1 and Ω_h^2 are two symmetric uniform quadrilateral meshes separated by a flat interface centered at $y = 0.5$ and with a gap of thickness $h^2/2$. The computational domains are similar to the ones illustrated in Fig. 5, although the gap used in the current example is smaller. Ω_h^1 denotes the bottom mesh and Ω_h^2 the upper one. Note that the area of the computational domain increases as the mesh is refined, which motivates the use of error norms divided by $|\Omega_h|^{1/2}$.

The gap $\delta = h^2/2$ is uniform on the interface and there is a one-to-one face bijection between the two interfaces; hence, $C_{nc} = 0$. Table 3 shows the errors and convergence rates for the approximate solution u_h, the approximate gradient $\boldsymbol{q}_h$ and the post-processed solution u_h^*. We observe that the HDG

TABLE 3 *History of convergence of the HDG method for a square domain with a flat interface and* $\delta = h^2/2$

k	Mesh size h	e_u	e.o.c.	$e_{\boldsymbol{q}}$	e.o.c.	e_{u^*}	e.o.c.
	5.000e−01	1.20e−01	—	3.57e−01	—	5.89e−02	—
	2.500e−01	4.55e−02	1.40	1.43e−01	1.33	9.93e−03	2.57
	1.250e−01	1.40e−02	1.70	4.44e−02	1.68	1.49e−03	2.73
1	6.250e−02	3.91e−03	1.84	1.24e−02	1.84	2.07e−04	2.85
	3.125e−02	1.03e−03	1.92	3.28e−03	1.92	2.72e−05	2.92
	1.562e−02	2.66e−04	1.96	8.43e−04	1.96	3.50e−06	2.96
	7.812e−03	6.74e−05	1.98	2.14e−04	1.98	4.43e−07	2.98
	5.000e−01	3.32e−02	—	1.61e−01	—	2.48e−02	—
	2.500e−01	4.01e−03	3.05	1.44e−02	3.49	1.43e−03	4.11
	1.250e−01	5.58e−04	2.85	1.80e−03	3.00	7.46e−05	4.26
2	6.250e−02	7.48e−05	2.90	2.37e−04	2.92	4.13e−06	4.18
	3.125e−02	9.69e−06	2.95	3.07e−05	2.95	2.41e−07	4.10
	1.562e−02	1.23e−06	2.97	3.90e−06	2.98	1.46e−08	4.05
	7.812e−03	1.55e−07	2.99	4.92e−07	2.99	8.94e−10	4.03
	5.000e−01	2.32e−03	—	1.12e−02	—	1.77e−03	—
	2.500e−01	2.12e−04	3.46	8.73e−04	3.69	1.29e−04	3.78
	1.250e−01	1.35e−05	3.97	4.63e−05	4.24	4.11e−06	4.98
3	6.250e−02	8.76e−07	3.95	2.82e−06	4.03	1.21e−07	5.08
	3.125e−02	5.61e−08	3.97	1.78e−07	3.98	3.63e−09	5.06
	1.562e−02	3.55e−09	3.98	1.13e−08	3.99	1.11e−10	5.04
	7.812e−03	2.23e−10	3.99	7.08e−10	3.99	3.13e−12	5.14
	5.000e−01	2.04e−03	—	1.13e−02	—	2.03e−03	—
	2.500e−01	1.78e−05	6.84	8.07e−05	7.12	1.37e−05	7.22
	1.250e−01	4.35e−07	5.36	1.43e−06	5.82	9.50e−08	7.17
4	6.250e−02	1.41e−08	4.94	4.47e−08	5.00	8.46e−10	6.81
	3.125e−02	4.52e−10	4.97	1.43e−09	4.97	9.31e−12	6.51
	1.562e−02	1.43e−11	4.98	4.56e−11	4.97	1.16e−13	6.33

approximation of u and $\boldsymbol{q}$ converges with order $k+1$ as predicted by Remark 4.4. We also observe an order of convergence of $k+2$ for the post-processed solution, which is better than the one stated in (4.8).

For the second test, we now consider that Ω_h^1 and Ω_h^2 are connected via noncoincident curved interfaces. The computational subdomains make use of isoparametric curved elements to represent two different curved interfaces. More specifically,

$$\mathcal{I}_h^1 \text{ interpolates the curve } y(x) = 0.5 + 0.025\sin(4\pi x),$$

$$\mathcal{I}_h^2 \text{ interpolates the curve } y(x) = 0.5 + \left(0.025 + h^2/2\right)\sin(4\pi x).$$

The two subdomains are similar to the ones illustrated in Fig. 6, although the shape of $\mathcal{I}_h^2$ is slightly different here. From the definitions of the computational interfaces, it is obvious that the two subdomains partially overlap and partially separate, with the width of both gaps and overlaps being bound by $h^2/2$. Assumption (A.3) is no longer exactly satisfied since the direction of the connecting segments

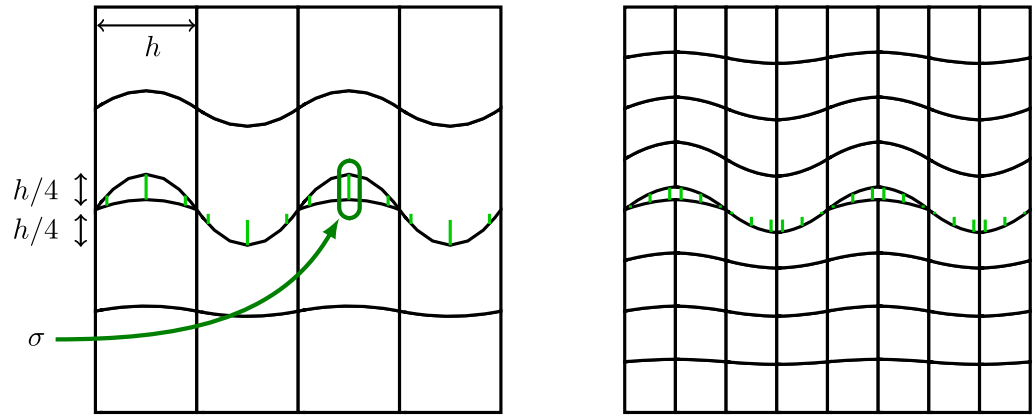

FIG. 6. Two of the meshes used for the fourth numerical example, with curved elements, $k = 2$ being displayed here. $h = 1/4$ for the left mesh and $h = 1/8$ for the right one. Note the length of the connecting segments is bounded by $h/4$, in both the overlap and the gap areas.

$\boldsymbol{m}$ deviates from the normal vectors. However, here, $1 - \boldsymbol{m} \cdot \boldsymbol{n}_1$ and $1 - \boldsymbol{m} \cdot \boldsymbol{n}_2$ remain small all along the computational interfaces. Note that no special treatment is applied in the overlapped regions, as the extrapolation operator (2.1) becomes a mere interpolation.

In Table 4, we show the results for this case and observe that the approximations of all the variables converge with order $k+1$, verifying Corollary 4.3, and the post-processed solution converges with order $k+2$. The results show that the HDG method provides optimal convergence even for partially overlapped and separated subdomains.

5.2 *Test cases with gap $\delta = \mathcal{O}(h)$*

We now consider two new numerical examples replicating the two first examples with wider mesh gaps. The third example is similar to the first one, but with a gap width now equal to $h/4$ as shown in Fig. 5. We present the numerical results in Table 5. Even though this scenario is not covered by our theory since now $r_e = 1/4$ and $\alpha = 0$, we observe that all the approximate variables still converge with the optimal order $k + 1$. However, the superconvergence of the post-processed solution is lost.

Finally, we set a fourth example similar to the second one by changing the definition of the computational interface

$$\mathcal{I}_h^2 \text{ interpolating the curve } y(x) = 0.5 + (0.025 + h/4)\sin(4\pi x),$$

such that now $\delta \leq h/4$. Since $\gamma = 0$, this case is not covered by the analysis. The computational domains are illustrated in Fig. 6. In Table 6, we show the results for this case and observe that the approximations of all the variables converge with order $k + 1$. Although there is not yet an analysis for the case $\delta = \mathcal{O}(h)$, it seems that our method provides optimal orders of convergence for the approximate solution and gradient.

TABLE 4 *History of convergence of the HDG method for a square domain with partially overlapping curved meshes and with* $\delta < h^2/2$

k	Mesh size h	e_u	e.o.c.	$e_{\boldsymbol{q}}$	e.o.c.	e_{u^*}	e.o.c.
1	5.000e−01	1.37e−01	—	3.68e−01	—	5.99e−02	—
	2.500e−01	4.68e−02	1.54	1.45e−01	1.35	1.11e−02	2.43
	1.250e−01	1.43e−02	1.71	4.57e−02	1.66	1.71e−03	2.70
	6.250e−02	3.96e−03	1.85	1.29e−02	1.83	2.39e−04	2.84
	3.125e−02	1.05e−03	1.92	3.49e−03	1.88	3.17e−05	2.91
	1.562e−02	2.70e−04	1.96	9.30e−04	1.91	4.13e−06	2.94
	7.812e−03	6.86e−05	1.98	2.46e−04	1.92	5.30e−07	2.96
2	5.000e−01	2.63e−02	—	8.43e−02	—	3.51e−03	—
	2.500e−01	5.22e−03	2.33	2.15e−02	1.97	6.01e−04	2.55
	1.250e−01	6.38e−04	3.03	2.50e−03	3.11	2.38e−05	4.66
	6.250e−02	8.48e−05	2.91	3.45e−04	2.86	1.42e−06	4.07
	3.125e−02	1.11e−05	2.93	4.69e−05	2.88	8.99e−08	3.98
	1.562e−02	1.42e−06	2.96	6.22e−06	2.91	5.75e−09	3.97
	7.812e−03	1.81e−07	2.98	8.08e−07	2.95	3.67e−10	3.97
3	5.000e−01	1.33e−02	—	1.51e−01	—	1.18e−02	—
	2.500e−01	4.50e−04	4.89	2.45e−03	5.95	6.51e−05	7.50
	1.250e−01	4.56e−05	3.30	2.62e−04	3.22	2.23e−06	4.87
	6.250e−02	3.17e−06	3.85	1.83e−05	3.84	6.16e−08	5.18
	3.125e−02	2.09e−07	3.92	1.23e−06	3.89	1.94e−09	4.99
	1.562e−02	1.35e−08	3.95	8.07e−08	3.93	6.13e−11	4.98
	7.812e−03	8.62e−10	3.97	5.19e−09	3.96	1.94e−12	4.98
4	5.000e−01	5.65e−03	—	4.76e−02	—	4.41e−03	—
	2.500e−01	2.31e−04	4.61	1.33e−03	5.17	3.87e−05	6.83
	1.250e−01	6.78e−06	5.09	3.58e−05	5.21	2.51e−07	7.27
	6.250e−02	1.92e−07	5.14	1.09e−06	5.04	3.77e−09	6.06
	3.125e−02	6.24e−09	4.95	3.62e−08	4.91	5.78e−11	6.03
	1.562e−02	2.00e−10	4.96	1.19e−09	4.93	9.08e−13	5.99

5.3 *Effect of the asymmetric transmission conditions*

The two transmission conditions (2.12) are obviously asymmetric, as they arbitrarily assign different roles to the mesh interfaces $\mathcal{I}_h^1$ and $\mathcal{I}_h^2$. The transmission conditions could also be swapped by using (2.16) instead. This short study assess the numerical difference between the two approaches.

For all the numerical examples studied so far, there is a one-to-one face bijection between the two interfaces. No mesh is finer than the other. On these examples, when using swapped condition (2.16), the errors are very similar and the estimated orders of convergence are identical. Therefore, the corresponding results are not reported here.

We now consider a case where the mesh symmetry is broken, with a bottom mesh Ω_h^1 twice as fine as the upper mesh Ω_h^2, as shown in Fig. 7. For this numerical example, we use simplex meshes, with a uniform gap width $\delta = h^2/2$. In Table 7, we observe that the errors behave quite differently when considering either transmission conditions (2.12) or (2.16). When conditions (2.12) are used, i.e., when

TABLE 5 *History of convergence of the HDG method for a square domain with a flat interface and* $\delta = h/4$

k	Mesh size h	e_u	e.o.c.	$e_{\boldsymbol{q}}$	e.o.c.	e_{u^*}	e.o.c.
1	5.000e−01	1.20e−01	—	3.57e−01	—	5.89e−02	—
	2.500e−01	4.43e−02	1.44	1.41e−01	1.34	8.95e−03	2.72
	1.250e−01	1.38e−02	1.69	4.42e−02	1.68	1.15e−03	2.96
	6.250e−02	3.88e−03	1.83	1.24e−02	1.83	2.63e−04	2.13
	3.125e−02	1.03e−03	1.91	3.30e−03	1.91	8.31e−05	1.66
	1.562e−02	2.66e−04	1.95	8.52e−04	1.96	2.40e−05	1.79
	7.812e−03	6.76e−05	1.98	2.16e−04	1.98	6.44e−06	1.90
2	5.000e−01	3.32e−02	—	1.61e−01	—	2.48e−02	—
	2.500e−01	4.96e−03	2.74	2.20e−02	2.87	3.46e−03	2.84
	1.250e−01	6.74e−04	2.88	2.79e−03	2.98	4.19e−04	3.05
	6.250e−02	8.83e−05	2.93	3.50e−04	2.99	5.02e−05	3.06
	3.125e−02	1.13e−05	2.96	4.39e−05	3.00	6.09e−06	3.04
	1.562e−02	1.43e−06	2.98	5.50e−06	3.00	7.49e−07	3.02
	7.812e−03	1.80e−07	2.99	6.88e−07	3.00	9.27e−08	3.01
3	5.000e−01	2.32e−03	—	1.12e−02	—	1.77e−03	—
	2.500e−01	4.03e−04	2.53	2.06e−03	2.45	3.72e−04	2.25
	1.250e−01	3.37e−05	3.58	1.71e−04	3.59	3.15e−05	3.56
	6.250e−02	2.35e−06	3.84	1.18e−05	3.85	2.20e−06	3.84
	3.125e−02	1.54e−07	3.93	7.72e−07	3.94	1.44e−07	3.93
	1.562e−02	9.84e−09	3.97	4.92e−08	3.97	9.19e−09	3.97
	7.812e−03	6.21e−10	3.99	3.10e−09	3.99	5.80e−10	3.99
4	5.000e−01	2.04e−03	—	1.13e−02	—	2.03e−03	—
	2.500e−01	4.85e−05	5.40	2.56e−04	5.46	4.74e−05	5.42
	1.250e−01	1.01e−06	5.58	5.10e−06	5.65	9.38e−07	5.66
	6.250e−02	2.32e−08	5.45	1.08e−07	5.56	1.90e−08	5.63
	3.125e−02	6.07e−10	5.26	2.59e−09	5.38	4.19e−10	5.50
	1.562e−02	1.73e−11	5.14	6.91e−11	5.23	9.97e−12	5.39

the numerical fluxes are connected on the coarse mesh, the flux approximation converges with the sub-optimal order $k + 1/2$, and the post-processed scalar variable converges with order $k + 1$. When the swapped conditions (2.16) are used, i.e., when the numerical fluxes are connected on the finer interface mesh, the optimal order of convergence $k+1$ is observed for all variables, and the post-processed solution superconverges with order $k+2$. Based on these observations, it seems that the numerical fluxes have to be connected on the finer mesh, which is also the approach followed in de Boer *et al.* (2007) and Chen & Cockburn (2012).

This last numerical experiment exemplifies the Remark 4.4. In general, the fact of not having a one-to-one face bijection between the two interfaces may deteriorate the convergence rate of the flux and the post-processed solution. Hence, according to Corollary 4.3, the guaranteed rates are $k + 1/2$ for the error of the flux and $k + 1$ for the error in the post-processing, which agrees with the rates reported in Table 7 for conditions (2.12).

TABLE 6 *History of convergence of the HDG method for a square domain with partially overlapping curved meshes and* $\delta \leq h/4$

k	Mesh size h	e_u	e.o.c.	$e_{\boldsymbol{q}}$	e.o.c.	e_{u^*}	e.o.c.
	5.000e−01	1.37e−01	—	3.68e−01	—	5.99e−02	—
	2.500e−01	4.68e−02	1.54	1.45e−01	1.35	1.11e−02	2.43
	1.250e−01	1.45e−02	1.69	4.70e−02	1.62	1.67e−03	2.74
1	6.250e−02	4.00e−03	1.86	1.32e−02	1.84	2.21e−04	2.92
	3.125e−02	1.05e−03	1.92	3.55e−03	1.89	2.83e−05	2.96
	1.562e−02	2.71e−04	1.96	9.42e−04	1.91	4.83e−06	2.55
	7.812e−03	6.87e−05	1.98	2.48e−04	1.93	1.25e−06	1.95
	5.000e−01	2.63e−02	—	8.43e−02	—	3.51e−03	—
	2.500e−01	6.69e−03	1.97	2.92e−02	1.53	1.07e−03	1.72
	1.250e−01	7.62e−04	3.13	3.29e−03	3.15	6.78e−05	3.98
2	6.250e−02	9.34e−05	3.03	4.08e−04	3.01	7.93e−06	3.10
	3.125e−02	1.17e−05	3.00	5.17e−05	2.98	1.02e−06	2.96
	1.562e−02	1.47e−06	2.99	6.59e−06	2.97	1.31e−07	2.96
	7.812e−03	1.84e−07	3.00	8.37e−07	2.98	1.67e−08	2.97
	5.000e−01	1.33e−02	—	1.51e−01	—	1.18e−02	—
	2.500e−01	8.88e−04	3.90	5.02e−03	4.92	1.74e−04	6.08
	1.250e−01	7.26e−05	3.61	4.00e−04	3.65	8.64e−06	4.33
3	6.250e−02	4.39e−06	4.05	2.49e−05	4.01	5.28e−07	4.03
	3.125e−02	2.51e−07	4.13	1.46e−06	4.09	3.57e−08	3.89
	1.562e−02	1.50e−08	4.07	8.90e−08	4.04	2.36e−09	3.92
	7.812e−03	9.14e−10	4.03	5.51e−09	4.02	1.52e−10	3.95
	5.000e−01	5.65e−03	—	4.76e−02	—	4.41e−03	—
	2.500e−01	3.51e−04	4.01	2.10e−03	4.51	9.08e−05	5.60
	1.250e−01	1.29e−05	4.76	7.14e−05	4.88	6.31e−07	7.17
4	6.250e−02	2.80e−07	5.53	1.60e−06	5.48	6.88e−09	6.52
	3.125e−02	7.62e−09	5.20	4.43e−08	5.17	8.82e−11	6.29
	1.562e−02	2.22e−10	5.10	1.31e−09	5.08	1.26e−12	6.13

6. Conclusions

We have proposed a novel high-order HDG method to compute an approximation of the solution of a PDE whose domain is discretized by a union of dissimilar meshes. This new technique is suitable to handle situations where a domain is divided by independently meshed subdomains. The HDG discretizations associated with each subdomain are tied together by appropriate transmission conditions across the dissimilar interfaces that allow the method to keep high-order accuracy for smooth enough solutions. Under closeness assumptions relating δ, the size of the gap between the dissimilar interfaces, and the meshsize, we theoretically proved that the method is well-posed and stable. Moreover, if the size of the gap is of order of $h^{1+\gamma}$ for all $\gamma \in (3/4, 1]$, we showed that the error of the method is of order h^{k+1} and $h^{k+1/2}$ for the scalar variable and its gradient, respectively. In addition, for the particular case where a face of a dissimilar interfaces is mapped one-to-one to a face of other interface, the error in both variables is of order h^{k+1}. Finally, we have provided a variety of numerical experiments illustrating that the method performs as predicted by our estimates, and also behaves optimally even in

TABLE 7 *History of convergence of the HDG method for the fifth numerical example involving a bottom mesh twice as fine as the upper mesh and* $\delta = h^2/2$

		Transmission conditions (2.12)						Swapped transmission conditions (2.16)					
k	Mesh size h	e_u	e.o.c.	$e_{\boldsymbol{q}}$	e.o.c.	e_{u^*}	e.o.c.	e_u	e.o.c.	$e_{\boldsymbol{q}}$	e.o.c.	e_{u^*}	e.o.c.
	5.000e−01	9.70e−02	—	2.59e−01	—	2.53e−02	—	9.01e−02	—	2.81e−01	—	4.79e−02	—
	2.500e−01	3.19e−02	1.60	7.35e−02	1.82	2.84e−03	3.16	3.12e−02	1.53	5.26e−02	2.42	6.22e−03	2.95
1	1.250e−01	8.58e−03	1.89	2.30e−02	1.68	3.71e−04	2.94	8.53e−03	1.87	1.17e−02	2.16	7.16e−04	3.12
	6.250e−02	2.20e−03	1.96	7.58e−03	1.60	5.25e−05	2.82	2.20e−03	1.96	2.84e−03	2.05	8.34e−05	3.10
	3.125e−02	5.56e−04	1.99	2.58e−03	1.55	7.91e−06	2.73	5.56e−04	1.98	7.01e−04	2.02	9.99e−06	3.06
	1.562e−02	1.40e−04	1.99	8.95e−04	1.53	1.26e−06	2.65	1.40e−04	1.99	1.75e−04	2.01	1.22e−06	3.03
	5.000e−01	2.71e−02	—	1.17e−01	—	1.87e−02	—	1.94e−02	—	6.84e−02	—	7.07e−03	—
	2.500e−01	3.21e−03	3.08	9.23e−03	3.67	1.07e−03	4.13	3.07e−03	2.66	6.26e−03	3.45	5.71e−04	3.63
2	1.250e−01	4.13e−04	2.96	1.15e−03	3.00	5.92e−05	4.17	4.11e−04	2.90	6.75e−04	3.21	4.80e−05	3.57
	6.250e−02	5.26e−05	2.97	1.81e−04	2.68	3.71e−06	4.00	5.26e−05	2.97	7.90e−05	3.09	3.29e−06	3.87
	3.125e−02	6.64e−06	2.99	3.02e−05	2.58	2.85e−07	3.70	6.64e−06	2.99	9.66e−06	3.03	2.12e−07	3.95
	1.562e−02	8.33e−07	2.99	5.19e−06	2.54	2.76e−08	3.37	8.33e−07	2.99	1.20e−06	3.01	1.34e−08	3.98
	5.000e−01	3.00e−03	—	1.53e−02	—	1.67e−03	—	7.64e−03	—	4.17e−02	—	7.21e−03	—
	2.500e−01	2.47e−04	3.60	7.88e−04	4.28	1.02e−04	4.03	3.25e−04	4.55	1.30e−03	5.00	2.34e−04	4.94
3	1.250e−01	1.62e−05	3.93	4.33e−05	4.19	4.15e−06	4.62	1.68e−05	4.28	4.03e−05	5.02	6.08e−06	5.27
	6.250e−02	1.03e−06	3.98	3.02e−06	3.84	1.82e−07	4.51	1.02e−06	4.04	1.73e−06	4.54	1.64e−07	5.21
	3.125e−02	6.45e−08	3.99	2.39e−07	3.66	9.13e−09	4.32	6.40e−08	4.00	9.63e−08	4.17	4.70e−09	5.13
	1.562e−02	4.04e−09	4.00	2.01e−08	3.58	5.04e−10	4.18	4.01e−09	4.00	5.84e−09	4.04	1.40e−10	5.07
	5.000e−01	2.02e−03	—	1.12e−02	—	1.99e−03	—	1.93e−03	—	1.14e−02	—	1.90e−03	—
	2.500e−01	2.26e−05	6.48	9.41e−05	6.90	1.59e−05	6.97	2.02e−05	6.58	1.09e−04	6.70	1.22e−05	7.28
4	1.250e−01	5.81e−07	5.28	1.47e−06	6.00	1.50e−07	6.73	5.78e−07	5.13	1.60e−06	6.09	1.36e−07	6.48
	6.250e−02	1.82e−08	4.99	4.37e−08	5.07	1.89e−09	6.31	1.83e−08	4.98	3.50e−08	5.52	2.13e−09	6.00
	3.125e−02	5.74e−10	4.99	1.60e−09	4.78	3.19e−11	5.89	5.74e−10	4.99	9.81e−10	5.16	3.37e−11	5.98
	1.562e−02	1.80e−11	4.99	6.45e−11	4.63	6.88e−13	5.54	1.80e−11	5.00	3.24e−11	4.92	4.57e−13	6.20

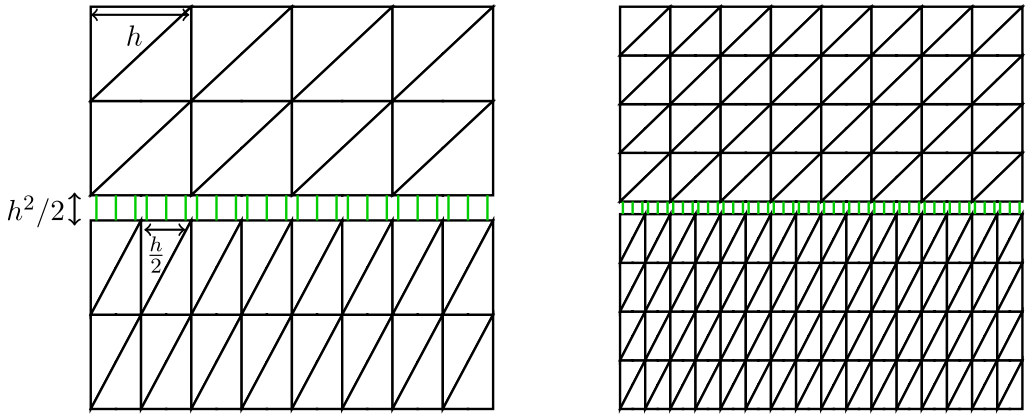

FIG. 7. Two of the meshes used for the fifth numerical example, obtained for $h = 1/4$ (left) and $h = 1/8$ (right). Each face of the top mesh is connected to two faces of the bottom mesh. The connecting segments at the Gauss points are drawn in green (here, $k = 2$). Note that, for visualization purposes, the gap displayed here is larger than the one actually used for the convergence study ($h^2/2$) in order to show the connecting segments.

cases not completely covered by our theory. These experiments suggest that the assumption $h^{1+\gamma}$ for all $\gamma \in (3/4, 1]$ could be relaxed and this is subject of a future work.

Funding

National Aeronautics and Space Administration (NNX16AP15A to S.T., N.-C.N. and J.P.); Chilean National Agency for Research and Development (Fondecyt 1200569 and Basal AFB170001 to M.S.).

REFERENCES

BFER, G. (1985) An isoparametric joint/interface element for finite element analysis. *Internat. J. Numer. Methods Engrg.*, **21**, 585–600.

DE BOER, A., VAN ZUIJLEN, A. & BIJL, H. (2007) Review of coupling methods for non-matching meshes. *Comput. Methods Appl. Mech. Engrg.*, **196**, 1515–1525. Domain decomposition methods: recent advances and new challenges in engineering.

CHEN, Y. & COCKBURN, B. (2012) Analysis of variable-degree HDG methods for convection-diffusion equations. Part I: general nonconforming meshes. *IMA J. Numer. Anal.*, **32**, 1267–1293.

CHEN, Y. & COCKBURN, B. (2014) Analysis of variable-degree HDG methods for convection-diffusion equations. Part II: semimatching nonconforming meshes. *Math. Comp.*, **83**, 87–111.

CHEUNG, J., GUNZBURGER, M., BOCHEV, P. & PEREGO, M. (2020) An optimally convergent higher-order finite element coupling method for interface and domain decomposition problems. *Results Appl. Math.*, **6**, 100094.

CHEUNG, J., PEREGO, M., BOCHEV, P. & GUNZBURGER, M. (2019) Optimally accurate higher-order finite element methods for polytopial approximations of domains with smooth boundaries. *Math. Comp.*, **88**, 2187–2219.

COCKBURN, B., GOPALAKRISHNAN, J. & SAYAS, F.-J. (2010) A projection-based error analysis of HDG methods. *Math. Comp.*, **79**, 1351–1367.

COCKBURN, B., QIU, W. & SHI, K. (2012) Conditions for superconvergence of HDG methods for second-order elliptic problems. *Math. Comp.*, **81**, 1327–1353.

COCKBURN, B., QIU, W. & SOLANO, M. (2014) *A priori* error analysis for HDG methods using extensions from subdomains to achieve boundary conformity. *Math. Comp.*, **83**, 665–699.

COCKBURN, B. & SOLANO, M. (2012) Solving Dirichlet boundary-value problems on curved domains by extensions from subdomains. *SIAM J. Sci. Comput.*, **34**, A497–A519.

COCKBURN, B. & SOLANO, M. (2014) Solving convection-diffusion problems on curved domains by extensions from subdomains. *J. Sci. Comput.*, **59**, 512–543.

DITTMANN, M., SCHUSS, S., WOHLMUTH, B. & HESCH, C. (2019) Weak c^n coupling for multipatch isogeometric analysis in solid mechanics. *Internat. J. Numer. Methods Engrg.*, **118**, 678–699.

DOHRMANN, C. R., KEY, S. W. & HEINSTEIN, M. (2000a) Methods for connecting dissimilar three-dimensional finite element meshes. *Internat. J. Numer. Methods Engrg.*, **47**, 1057–1080.

DOHRMANN, C. R., KEY, S. W. & HEINSTEIN, M. W. (2000b) A method for connecting dissimilar finite element meshes in two dimensions. *Internat. J. Numer. Methods Engrg.*, **48**, 655–678.

FLEMISCH, B., MELENK, J. & WOHLMUTH, B. (2005a) Mortar methods with curved interfaces. *Appl. Numer. Math.*, **54**, 339–361. Selected papers from the 16th Chemnitz Finite Element Symposium 2003.

FLEMISCH, B., PUSO, M. A. & WOHLMUTH, B. I. (2005b) A new dual mortar method for curved interfaces: 2D elasticity. *Internat. J. Numer. Methods Engrg.*, **63**, 813–832.

FLEMISCH, B. & WOHLMUTH, B. I. (2007) Stable Lagrange multipliers for quadrilateral meshes of curved interfaces in 3D. *Comput. Methods Appl. Mech. Engrg.*, **196**, 1589–1602. Domain decomposition methods: recent advances and new challenges in engineering.

HEINSTEIN, M. & LAURSEN, T. (2003) A three dimensional surface-to-surface projection algorithm for non-coincident domains. *Comm. Numer. Methods Engrg.*, **19**, 421–432.

HUYNH, L. T., NGUYEN, N., PERAIRE, J. & KHOO, B. (2013) A high-order hybridizable discontinuous Galerkin method for elliptic interface problems. *Internat. J. Numer. Methods Engrg.*, **93**, 183–200.

LAURSEN, T. A. & HEINSTEIN, M. W. (2003) Consistent mesh tying methods for topologically distinct discretized surfaces in non-linear solid mechanics. *Internat. J. Numer. Methods Engrg.*, **57**, 1197–1242.

LENOIR, M. (1986) Optimal isoparametric finite elements and error estimates for domains involving curved boundaries. *SIAM J. Numer. Anal.*, **23**, 562–580.

QIU, W., SOLANO, M. & VEGA, P. (2016) A high order HDG method for curved-interface problems via approximations from straight triangulations. *J. Sci. Comput.*, **69**, 1384–1407.

STENBERG, R. (1991) Postprocessing schemes for some mixed finite elements. *ESAIM Math. Model. Numer. Anal.*, **25**, 151–167.

Appendix

Proof of Lemma 2.1.

Proof. By a density argument, it is enough to show the first three estimates assuming $\psi \in C^\infty \cap H^2(\Omega)$. First, let $e \in \mathcal{I}_h^2$ and $\boldsymbol{x}_2$. By Taylor's theorem, we write

$$\psi(\boldsymbol{x}_2) = \psi(\boldsymbol{\phi}(\boldsymbol{x}_2)) + |\sigma(\boldsymbol{x}_2)|\partial_{\boldsymbol{n}_2}\psi(\boldsymbol{\phi}(\boldsymbol{x}_2)) + R_\psi(\boldsymbol{x}_2), \tag{A.1}$$

where the residual is given by $R_\psi(\boldsymbol{x}_2) := \int_0^{|\sigma(\boldsymbol{x}_2)|}(\sigma(\boldsymbol{x}_2)-s)\partial^2_{\boldsymbol{n}_2}\psi(\boldsymbol{x}_1+s\boldsymbol{n}_2)\,\mathrm{d}s$. By the Cauchy–Schwarz inequality, it is possible to obtain that $|R_\psi(\boldsymbol{x}_2)|^2 \leq \frac{|\sigma(\boldsymbol{x}_2)|^3}{3}\|\partial^2_{\boldsymbol{n}_2}\psi\|^2_{L^2(0,|\sigma(\boldsymbol{x}_2)|)}$. Then, since $\boldsymbol{\varphi} = -\nabla\psi$, from (A.1), we deduce

$$\Big(|\sigma(\boldsymbol{x}_2)|^{-1/2}(\psi(\boldsymbol{x}_2) - \psi(\boldsymbol{\phi}(\boldsymbol{x}_2)) + |\sigma(\boldsymbol{x}_2)|^{1/2}\boldsymbol{\varphi}(\boldsymbol{\phi}(\boldsymbol{x}_2))\cdot\boldsymbol{n}_2)\Big)^2 \leq \frac{|\sigma(\boldsymbol{x}_2)|^2}{3}\|\partial^2_{\boldsymbol{n}_2}\psi\|^2_{L^2(0,|\sigma(\boldsymbol{x}_2)|)}.$$

Integrating this expression along e and bounding the norm of the second derivatives by the H^2-norm, we obtain

$$\| |\sigma|^{-1/2}(\psi - \psi \circ \boldsymbol{\phi}) + |\sigma(\boldsymbol{x}_2)|^{1/2}(\boldsymbol{\varphi} \circ \boldsymbol{\phi}) \cdot \boldsymbol{n}_2) \|_e^2 \leq \frac{1}{3} \max_{\boldsymbol{x^2} \in e} |\sigma(\boldsymbol{x}_2)|^2 \ \|\psi\|^2_{H^2(\Omega)}.$$

Thus, since $|\sigma(\boldsymbol{x}_2)| \leq R_2 h_2$, for all $\boldsymbol{x}_2 \in e$, (2.10a) follows. Similarly, from (A.1), we can bound

$$\begin{aligned} ||\sigma(\boldsymbol{x}_2)|^{-1/2}(\psi(\boldsymbol{x}_2) - \psi(\boldsymbol{\phi}(\boldsymbol{x}_2)))|^2 &\leq 2|\sigma(\boldsymbol{x}_2)| \ |\partial_{\boldsymbol{n^2}} \psi(\boldsymbol{\phi}(\boldsymbol{x}_2))|^2 + 2|\sigma(\boldsymbol{x}_2)|^{-1} |R_\psi(\boldsymbol{x}_2)|^2 \\ &\leq 2|\sigma(\boldsymbol{x}_2)| \ |\partial_{\boldsymbol{n}_2} \psi(\boldsymbol{\phi}(\boldsymbol{x}_2))|^2 + \frac{2}{3} |\sigma(\boldsymbol{x}_2)|^2 \|\partial^2_{\boldsymbol{n}_2} \psi\|^2_{L^2(0,|\sigma(\boldsymbol{x}_2)|)}, \end{aligned}$$

where, for the last step, we have used the fact that $\boldsymbol{\varphi} = -\nabla\psi$. Thus, integrating previous expression over e, considering that $|\sigma(\boldsymbol{x}_2)|^2 \leq |\sigma(\boldsymbol{x}_2)|$ and bounding the norm of the second derivatives by the H^2-norm, we conclude

$$\| |\sigma(\boldsymbol{x}_2)|^{-1/2}(\psi(\boldsymbol{x}_2) - \psi(\boldsymbol{\phi}(\boldsymbol{x}_2)))\|_e^2 \lesssim \max_{\boldsymbol{x^2} \in e} |\sigma(\boldsymbol{x}_2)| \ \|\psi\|^2_{H^2(\Omega)},$$

which implies (2.10a), since $\max_{\boldsymbol{x^2} \in e} |\sigma(\boldsymbol{x}_2)| \leq \delta$. Now, to show (2.10c), again by Taylor's theorem, we write

$$\boldsymbol{\varphi}(\boldsymbol{x}_2) \cdot \boldsymbol{n^2} = \boldsymbol{\varphi}(\boldsymbol{\phi}(\boldsymbol{x}_2)) \cdot \boldsymbol{n}_2 + R_{\boldsymbol{\varphi}}(\boldsymbol{x}_2),$$

where $R_{\boldsymbol{\varphi}}(\boldsymbol{x}_2) := \int_0^{|\sigma(\boldsymbol{x}_2)|} \partial_{\boldsymbol{n}_2}(\boldsymbol{\varphi}(\boldsymbol{x}_1 + s\boldsymbol{n}_2) \cdot \boldsymbol{n}_2) \, \mathrm{d}s$. The estimate in (2.10c) follows by the same arguments employed before and noticing that $|R_{\boldsymbol{\varphi}}(\boldsymbol{x}_2)|^2 \leq |\sigma(\boldsymbol{x}_2)| \|\partial_{\boldsymbol{n}_2}(\boldsymbol{\varphi} \cdot \boldsymbol{n^2})\|^2_{L^2(0,|\sigma(\boldsymbol{x}_2)|)}$.

Finally, let $F \in \mathcal{F}_h^2$, $e = \boldsymbol{\phi}(F) \in \mathcal{I}_h^1$, K_e the element where e belongs and $p \in \mathbb{P}_k(K_e)$. By repeating the same arguments as above, for $\boldsymbol{x}_2 \in F$ it is possible to deduce that

$$|p(\boldsymbol{x}_2) - p(\boldsymbol{\phi}(\boldsymbol{x}_2))|^2 \leq |\sigma(\boldsymbol{x}_2)| \ \|\nabla p\|^2_{L^2(0,|\sigma(\boldsymbol{x}_2)|)}.$$

Integrating along F, noticing that $|\sigma(\boldsymbol{x}_2)| \leq \delta_e$ and recalling the definition of K_e^{ext} in (2.4), we have

$$\|p - p \circ \boldsymbol{\phi}\|_F^2 \leq \delta_e \ \|\nabla p\|^2_{K_e^{ext}} \leq (C_e^{ext})^2 \ \delta_e r_e \ h_{K_e}^{-2} \ \|p\|^2_{K_e} \lesssim (C_e^{ext})^2 \ \delta_e^2 \ h_e^{-3} \ \|p\|^2_{K_e},$$

where we used the definition of C_e^{ext} (cf. (2.7)) and the inverse inequality on K_e. □